SEISMIC RESPONSE OF LIGHT INTERNAL EQUIPMENT IN BASE ISOLATED STRUCTURES

by

James M. Kelly
Professor of Civil Engineering
University of California, Berkeley

Hsiang-Chuan Tsai
Graduate Student in Civil Engineering
University of California, Berkeley

Division of Structural Engineering and Structural Mechanics
Department of Civil Engineering
College of Engineering
University of California, Berkeley

September 1984

Abstract

The seismic response of light secondary systems in a building is dependent on the response of the primary structural system to the seismic ground motion with the result that very high accelerations can be induced in such secondary systems. This response can be reduced through the use of aseismic base isolation which is a design strategy founded on the premise that the entire building can be decoupled from the damaging horizontal components of seismic ground motion by use of some form of isolation system.

The paper presents a theoretical analysis of this phenomenon and a parallel experimental program which show that the use of base isolation can not only attenuate the response of the primary structural system but also reduce the response of secondary systems. Thus, the design of equipment and piping in a base-isolated building is very much simpler than that for a conventionally founded structure: inelastic response and equipment-structure interaction need not be considered and multiple support response analysis is rendered unnecessary.

Although an isolation system with linear elastic bearings can reduce the acceleration of the structure, it may be accompanied by large relative displacements between the structure and the ground. A system using lead-rubber hysteretic bearings, having a force-displacement relation which is approximately a bilinear loop, can reduce these displacements depending on the design earthquakes. The experimental results show that these bearings can dissipate energy and limit the displacement and acceleration of the structure but are less effective in reducing the accelerations in the internal equipment.

The results of both the analysis and the tests show that base isolation is a very effective method for the seismic protection of light equipment items in buildings.

Acknowledgments

The research reported here was sponsored in part by the National Science Foundation under grant no. CEE-82113604. The bearings for the experiments were manufactured by Oil States Industries Inc., Athens, Texas.

Table of Contents

List of Tables

List of Figures

Chapter 1 INTRODUCTION

Earthquake loading is unique among the types of forces to which a building may be subjected. The essential feature of this loading is that external load is applied directly to the structure only through its base. Forces developed at the upper levers are a consequence only of the local acceleration which results from the earthquake motion introduced at the base. The magnitude of the story acceleration is directly dependent upon the stiffness properties of structure. Thus, under the same earthquake, structures designed by different philosophies will be subjected to different earthquake loadings and have different responses.

The current design approach is to ensure that the structure has sufficient strength to sustain the forces induced by a moderate earthquake and has sufficient ductility under a strong earthquake. Ductility allows the structure to develop inelastic hinges at beam ends during strong ground motion. These hinges provide not only increased flexibility but also energy absorbing capacity, both of which help to limit the earthquake generated forces. However, such inelastic deformations require large interstory displacements and cause progressive breakdown of the structural components as well as damage to mounted secondary systems and non-structural components. Moreover, a structure strengthened to resist earthquake attack becomes more rigid and a larger amplification of the ground acceleration at each floor level may result. Thus, even if the structural members remain in the elastic range under a moderate earthquake, the secondary systems may be more severely damaged and the danger to occupants increased.

Base isolation is a different antiseismic design strategy. In this approach, a system of some kind is used to decouple the superstructure from the ground so that the damaging horizontal components of earthquake ground motion cannot be transmitted into the building. In general, an isolation system is equipped both with flexibility and an energy-absorbing capacity. Flexibility in the horizontal direction will lower the fundamental frequency of the structure to below the range of frequencies which dominate in the general earthquake input, so that the earthquake-induced loading will be decreased. However, the low stiffness of the isolation system could cause the displacements of the building to become too large. Hence, the isolation

system should have some energy-absorbing capacity which in addition to attenuating the transmission of energy into the building will also reduce the structural displacement. If the energy-absorbing mechanism involves inelastic behavior, this will be confined to the base isolation system and the damage during an earthquake can thus be confined to the isolation system and not to the structural members. Such damage will not cause severe harm to the secondary systems and occupants.

Many unimplemented base isolation systems have been proposed, but the concept has become a practical reality in recent years with the development of multilayer elastomeric bearings.[1] These bearings consist of thin sheets of rubber bonded to interleaving steel plates, so that they have sufficient vertical rigidity to sustain vertical loading and sufficient horizontal flexibility to isolate the building from the horizontal components of ground motion.

Many buildings such as hospitals, power plants, telephone exchanges, and pumping stations for water or gas pipelines contain essential equipment which must be designed to be integral with the primary structure under the earthquake-induced loading and must continue to operate in the aftermath of a severe earthquake. Since these internal equipment items are connected to the primary structure and driven by the structure during seismic motion, it is possible that very high accelerations could be induced in them. A further complication arises when the equipment has a natural frequency close to one of the natural frequencies of the primary structure, a situation referred to as tuning and one almost inevitable in a large system. Current design practices account for this possibility by permitting inelastic action in the equipment and its supports or by using energy-absorbing restrainers in the system. These, however, will make the design of such buildings more complicated and expensive.

Base isolation can solve this difficulty by constructing the entire building on a base isolation system. To evaluate the effect of base isolation on equipment response, an earlier series of experiments has been carried out on the large-scaled shaking table at Earthquake Simulator Laboratory of Earthquake Engineering Research Center, University of California, Berkeley.[2] In these tests, there were three forms of base isolation system; a fully isolating system with rubber

bearing only, a fail-safe skid isolating system and an energy-absorbing isolating system.

The fail-safe skid system consists of rubber bearings and skid systems.[3] and serves a dual purpose. The first of these purpose is to act as a fail-safe system. In the event of unexpectedly large relative displacements, which could cause the bearings to fail, the system would not collapse but would be caught on the skid system. The second purpose of the skid system is to function as a Coulomb friction damper. After the base floor girders and the skids come into contact at a certain value of relative horizontal displacement, a shearing force due to friction is developed in the skids, and in addition vertical load is transferred from the bearings to the skids. This has the effect of limiting the maximum displacement.

The energy-absorbing system used in these earlier tests consists of rubber bearings and tapered cantilever beams.[4] These beams are made of hot-rolled, low carbon mild steel and act as hysteretic dampers. For small deformation, the steel beams are elastic and become high stiffness members which reduce the structural displacement. But under more intense excitation, the steel beams yield and produce large hysteresis loops as the structure oscillates. The stiffness of the system drops dramatically and thus the effective frequency is reduced. Simultaneously their high energy absorption capacity is developed and very high effective damping is introduced.

The lead-rubber hysteretic bearing is another type of energy-absorbing isolating system recently developed. A four story reinforced concrete building using this type of isolating system has been designed and constructed in New Zealand.[5] The lead-rubber bearing consists of a rubber bearing with a lead plug inserted in its center. The lead plug acts as a hysteretic damper. It can provide a high stiffness to the bearing before yielding of the lead and form large hysteresis loops after yielding. Thus, the lead-rubber bearing can produce the required amount of damping by the selection of the appropriate size of lead plug.

In a recent test series, a five story steel frame mounted on the lead-rubber bearings has been tested on the shaking table and experimental results on the frame response have been reported.[6] As an additional feature of this test series, oscillators representing light equipment

Chapter 2 LEAD-RUBBER HYSTERETIC BEARING

2.1 Characteristics of Lead-Rubber Bearing

The lead-rubber bearing is a steel-reinforced multilayer elastomeric bearing with a hole in its center to facilitate the insertion of a lead plug as shown on Figure 1. The lead plug is firmly pressed into the hole and the lead forms a positive key between the steel plates within the bearing. Thus, when the elastomeric bearing is deformed horizontally, the lead insert is forced by the interlocking steel plates to deform over its whole volume in pure shear. In a single compact unit, the lead-rubber bearing provides the combined features of vertical load support, horizontal flexibility and energy absorbing capacity required for the base isolation of structures from earthquake attack and also prevents movement of the building under wind loading.

There are some reasons for choosing lead as the material for the insert in the bearings.[7] First, lead yields in shear at the relatively low stress of about 1.4 ksi and behaves approximately as an elastic-plastic solid. Thus a reasonable size insert can produce the necessary hysteresis damping force for the base isolation system. Second, at ambient temperature when lead is plastically deformed it is being 'hot worked' and the mechanical properties of the lead are being continuously restored by the interrelated processes of recovery, recrystallization and grain growth which are occurring simultaneously. Lead therefore has good fatigue properties during cycling at plastic strains. Third, because of its use in batteries, lead is readily available at the high purity of 99.9 per cent required for its mechanical properties to be predictable.

The relation between the shear force and shear displacement of lead-rubber bearing can be expressed approximately by the bilinear loop as shown on Figure 2. In small ground motion, the lead plug does not yield and provides a high stiffness to the elastomeric bearing. As the intensity of the motion increases, the stiffness of the bearing drops to that produced by the elastomer. Large hysteresis loops are formed due to yielding of the lead and significant energy dissipation occurs. Thus, the lead plug acts as a mechanical fuse and energy dissipator in the lead-rubber hysteretic bearing.

items were attached to the structural model to assess the influence of the lead plug bearings on the seismic response of light equipment items. These experimental results will be presented here for the first time. In order to understand the efficiency of the lead-rubber bearings, the other two kinds of foundation system, fixed base system and base-isolated system with the plain rubber bearings, have also been tested. The response of oscillators on these three kinds of foundation system are compared and discussed in the paper.

In addition, in this paper the theoretical response of the tuned equipment on the base-isolated structure is approximately derived using a mass-lumped mathematical model. The bearing in this model is assumed to be elastic and thus the model is entirely linear. The behavior of tuned light equipment in a base-isolated structure can be studied using this model to a high degree of accuracy when plain bearings are used and approximately in the case of lead plug bearings.

The correlations between the experiment results and the response of the mathematical model are made and discussed for the fixed base system and the base-isolated system with the plain rubber bearings. The response spectrum method is applied to calculate the response of the mathematical model and modal damping ratio is required by this method. Thus, in order to make a good correlation, a rational method is needed to evaluate the modal damping ratios from the bearing damping and the structural damping, and this is also developed in the paper.

easily solved.

To study the correlation between experimental results and the computer simulation, a two dimensional frame isolated on the bilinear bearings was analyzed by this computer program. The base displacements and base shear forces determined from the experiments and calculated from the computer program are compared in Figure 5 through Figure 7. Since the hysteresis loops of lead bearing after yielding are similar to the bilinear loop, the larger responses are matched very well. There are however some differences in the small response. Small hysteresis loops are found in the experiment even if the bearings have not reached the yield level. This does not occur in the bilinear model. It will remain in the linear elastic state, so that the energy dissipation is less and the calculated response is larger than in the experiment for small deformation.

2.2 Shaking Table Test and Numerical Correlation

A series of experiments have been carried out on the large-scaled shaking table to study the dynamic behavior of structures using the lead-rubber bearing isolation system and to compare with system which uses plain rubber bearing without lead.[6] The experimental model was a five-story steel frame mounted on the four bearings and was excited by several different earthquake inputs derived from historical earthquake records.

The test results show that the accelerations experienced by the frame on the lead-filled bearing are always less than the input acceleration. They are higher than for the unfilled bearing condition, but the relative displacements are lower. In contrast to the unfilled bearing case in which the frame responded almost as a rigid body, the peak accelerations of each floor for the lead-filled case do not occur simultaneously. The hysteresis loops for the unfilled bearing and lead-filled bearing are shown on Figure 3 and Figure 4. Large hysteresis loops in the lead-filled bearing are indicative of efficient energy dissipation.

Since the lead is nonlinear in its response, the magnitude of frame response is not proportional to that of input. The increased input intensity is accompanied with the increased isolation. In principle, a permanent deformation after yielding is possible. The nonlinearity also implies that the response should be dependent on previous history of bearing deformation. In fact, no severe permanent deformation was observed after a test and there was no dependence on previous history.

A computer program for the stress analysis of base-isolated structures has been developed at the University of California, Berkeley.[8] In this program, the bearing can be modeled to have a bilinear force-displacement relation, so that the effect of the energy-absorbing mechanism on the isolated structure can be calculated. The number of degrees of freedom for the superstructure, which is elastic, is reduced in this program by static condensation and the total number of degrees of freedom used in the nonlinear iteration is greatly reduced and the computing effort minimized. Because the program performs three dimensional analysis on the superstructure using the substructure concept, torsional response of the structure on the nonlinear bearings is

where Y_i is the generalized coordinate representing the amplitude of the i'th vibration mode and $\boldsymbol{\phi}_i$ is the vector of the respective mode shape. The mode shapes have the orthogonality properties,

$$\boldsymbol{\phi}_i^T \mathbf{M} \boldsymbol{\phi}_j = 0 \; ; \quad \boldsymbol{\phi}_i^T \mathbf{K} \boldsymbol{\phi}_j = 0 \quad \text{for } i \neq j \tag{3.7}$$

These lead Eq. (3.1) to be decoupled as

$$\ddot{Y}_i + \omega_i^2 Y_i = - L_i \ddot{u}_g \quad \text{for } i=1, \ldots, 5 \tag{3.8}$$

in which the various modal properties are defined as follows:

Generalized mass

$$M_i = \boldsymbol{\phi}_i^T \mathbf{M} \boldsymbol{\phi}_i \tag{3.9}$$

Modal frequency

$$\omega_i = \left(\frac{\boldsymbol{\phi}_i^T \mathbf{K} \boldsymbol{\phi}_i}{M_i} \right)^{1/2} \tag{3.10}$$

Participation factor

$$L_i = \frac{\boldsymbol{\phi}_i^T \mathbf{M} \mathbf{r}}{M_i} \tag{3.11}$$

3.2 Dynamic Behavior of Base-Isolated Structure

The theoretical model of the base-isolated structure is shown on Figure 9. The base of the isolated structure is taken to be a lumped mass m_b on a spring of stiffness k_b. Let u_b be the base displacement relative to the ground and u_i be the i'th floor displacement relative to the base, which is the deformation of superstructure and equivalent to the floor displacement relative to the ground in the case of the fixed base structure. The undamped equations of motion subjected to a ground acceleration $\ddot{u}_g$ are expressed by

$$\bar{\mathbf{M}} \ddot{\bar{\mathbf{u}}} + \bar{\mathbf{K}} \bar{\mathbf{u}} = - \bar{\mathbf{M}} \bar{\mathbf{r}} \ddot{u}_g \tag{3.12}$$

Chapter 3 MATHEMATICAL ANALYSIS OF ELASTIC MODELS

3.1 Basic Equations of Fixed Base Structure

A fixed base model of five stories is shown on Figure 8, which has the lumped mass m_i and stiffness k_i on the i'th floor. When this model is subjected to a ground acceleration $\ddot{u}_g$, its undamped equations of motion can be written as

$$\mathbf{M}\ddot{\mathbf{u}} + \mathbf{K}\mathbf{u} = -\mathbf{M}\mathbf{r}\ddot{u}_g \tag{3.1}$$

where $\mathbf{M}$ is the mass matrix, defined as

$$\mathbf{M} = \begin{bmatrix} m_1 & 0 & 0 & 0 & 0 \\ 0 & m_2 & 0 & 0 & 0 \\ 0 & 0 & m_3 & 0 & 0 \\ 0 & 0 & 0 & m_4 & 0 \\ 0 & 0 & 0 & 0 & m_5 \end{bmatrix} \tag{3.2}$$

$\mathbf{K}$ is the stiffness matrix, defined as

$$\mathbf{K} = \begin{bmatrix} k_1+k_2 & -k_2 & 0 & 0 & 0 \\ -k_2 & k_2+k_3 & -k_3 & 0 & 0 \\ 0 & -k_3 & k_3+k_4 & -k_4 & 0 \\ 0 & 0 & -k_4 & k_4+k_5 & -k_5 \\ 0 & 0 & 0 & -k_5 & k_5 \end{bmatrix} \tag{3.3}$$

$\mathbf{r}$ is the displacement influence vector, defined as

$$\mathbf{r} = [1 \;\; 1 \;\; 1 \;\; 1 \;\; 1]^T \tag{3.4}$$

$\mathbf{u}$ is the relative displacement vector with the components as

$$\mathbf{u} = [u_1 \;\; u_2 \;\; u_3 \;\; u_4 \;\; u_5]^T \tag{3.5}$$

and $\ddot{\mathbf{u}}$ is the relative acceleration vector.

By the mode superposition method, the displacement can be expressed as

$$\mathbf{u} = \sum_{i=1}^{5} Y_i \boldsymbol{\phi}_i \tag{3.6}$$

$$\mathbf{u} \approx Y_1\boldsymbol{\phi}_1 + Y_2\boldsymbol{\phi}_2 \tag{3.19}$$

After substituting Eq. (3.19) into Eq. (3.17) and (3.18) and multiplying $\boldsymbol{\phi}_1^T$ and $\boldsymbol{\phi}_2^T$ to Eq. (3.18) respectively, the equations of motion can be simplified using the orthogonality properties in Eq. (3.7) and the modal properties in Eq. (3.9) to (3.11) to take the form

$$\begin{bmatrix} m_f & M_1L_1 & M_2L_2 \\ M_1L_1 & M_1 & 0 \\ M_2L_2 & 0 & M_2 \end{bmatrix} \begin{Bmatrix} \ddot{u}_b \\ \ddot{Y}_1 \\ \ddot{Y}_2 \end{Bmatrix} + \begin{bmatrix} k_b & 0 & 0 \\ 0 & M_1\omega_1^2 & 0 \\ 0 & 0 & M_2\omega_2^2 \end{bmatrix} \begin{Bmatrix} u_b \\ Y_1 \\ Y_2 \end{Bmatrix} = -\begin{Bmatrix} m_f \\ M_1L_1 \\ M_2L_2 \end{Bmatrix} \ddot{u}_g \tag{3.20}$$

This is a generalized equation of motion in terms of generalized coordinates u_b, Y_1 and Y_2. Although it is similar to Eq. (3.12), the number of degrees of freedom has been reduced.

The frequency of the i'th mode of the isolated structure will be denoted by $\bar{\omega}_i$ which with its mode shape can be found by solving the following eigenvalue problem,

$$\begin{bmatrix} \omega_b^2 & 0 & 0 \\ 0 & \omega_1^2 & 0 \\ 0 & 0 & \omega_2^2 \end{bmatrix} \begin{Bmatrix} \bar{u}_b^{(i)} \\ \bar{Y}_1^{(i)} \\ \bar{Y}_2^{(i)} \end{Bmatrix} = \bar{\omega}_i^2 \begin{bmatrix} 1 & R_1L_1 & R_2L_2 \\ L_1 & 1 & 0 \\ L_2 & 0 & 1 \end{bmatrix} \begin{Bmatrix} \bar{u}_b^{(i)} \\ \bar{Y}_1^{(i)} \\ \bar{Y}_2^{(i)} \end{Bmatrix} \tag{3.21}$$

in which $R_1 = \dfrac{M_1}{m_f}$, $R_2 = \dfrac{M_2}{m_f}$ and $\omega_b = \sqrt{\dfrac{k_b}{m_f}}$.

In general, the stiffness of the isolation level, k_b, is much less than that of the various superstructural levels; in other words, $\omega_b^2 << \omega_1^2$. Thus, the value of $\epsilon = (\dfrac{\omega_b}{\omega_1})^2$ is very small. Also, if the modal frequencies of the fixed base structure are well spaced, it is reasonable to assume that $(\dfrac{\omega_1}{\omega_2})^2$ has the same order of ϵ. If the terms having an order higher than ϵ are neglected, the approximate values of the isolated modal frequencies can be derived as

$$\bar{\omega}_1 \approx \omega_b \tag{3.22}$$

$$\bar{\omega}_2 \approx \frac{1}{\sqrt{1-P_1}}\omega_1\left[1+\frac{P_1}{2}(\frac{\omega_b}{\omega_1})^2-\frac{P_1P_2}{2(1-P_1)^2}(\frac{\omega_1}{\omega_2})^2\right] \tag{3.23}$$

$$\bar{\omega}_3 \approx \sqrt{\frac{1-P_1}{1-P_1-P_2}}\omega_2\left[1+\frac{P_1P_2}{2(1-P_1)}(\frac{\omega_1}{\omega_2})^2\right] \tag{3.24}$$

where

$$\overline{\mathbf{M}} = \begin{bmatrix} m_f & m_1 & m_2 & m_3 & m_4 & m_5 \\ m_1 & m_1 & 0 & 0 & 0 & 0 \\ m_2 & 0 & m_2 & 0 & 0 & 0 \\ m_3 & 0 & 0 & m_3 & 0 & 0 \\ m_4 & 0 & 0 & 0 & m_4 & 0 \\ m_5 & 0 & 0 & 0 & 0 & m_5 \end{bmatrix} \tag{3.13}$$

in which $m_f = m_b + m_1 + m_2 + m_3 + m_4 + m_5$;

$$\overline{\mathbf{K}} = \begin{bmatrix} k_b & 0 & 0 & 0 & 0 & 0 \\ 0 & k_1+k_2 & -k_2 & 0 & 0 & 0 \\ 0 & -k_2 & k_2+k_3 & -k_3 & 0 & 0 \\ 0 & 0 & -k_3 & k_3+k_4 & -k_4 & 0 \\ 0 & 0 & 0 & -k_4 & k_4+k_5 & -k_5 \\ 0 & 0 & 0 & 0 & -k_5 & k_5 \end{bmatrix} \tag{3.14}$$

$$\bar{\mathbf{r}} = [1 \ 0 \ 0 \ 0 \ 0 \ 0]^T \tag{3.15}$$

$$\bar{\mathbf{u}} = [u_b \ u_1 \ u_2 \ u_3 \ u_4 \ u_5]^T \tag{3.16}$$

By matrix partition, Eq. (3.12) can be rewritten in terms of the matrices **M**, **K**, **r** and **u** which have been defined in Eq. (3.2) to (3.5),

$$m_f \ddot{u}_b + (\mathbf{Mr})^T \ddot{\mathbf{u}} + k_b u_b = -m_f \ddot{u}_g \tag{3.17}$$

$$\mathbf{Mr}\,\ddot{u}_b + \mathbf{M}\ddot{\mathbf{u}} + \mathbf{K}\mathbf{u} = -\mathbf{Mr}\,\ddot{u}_g \tag{3.18}$$

These are the coupled equations of base and superstructure. The deformation of superstructure, **u**, can be expressed in terms of the fixed base mode shapes as defined in Eq. (3.6). In general, the contribution of higher superstructural modes to the deformation of superstructure is much less than that of the lower modes. In order to get the closed-form solution of the frequencies and mode shapes of the base-isolated structure, it is necessary to keep the number of degrees of freedom in the eigenvalue problem no more than three. Thus, neglecting the contribution of higher modes, the vector **u** is approximately expressed as the combination of the first two fixed base mode shapes,

the contribution of superstructural properties dominates in the higher modes of the base-isolated structure.

The participation factors can be formulated from the equation of motion in Eq. (3.20). According to the generalized mode shapes in Eq. (3.25) to (3.27), the participation factors are derived approximately equal to

$$\bar{L}_1 \approx 1-P_1(\frac{\omega_b}{\omega_1})^2 \tag{3.28}$$

$$\bar{L}_2 \approx P_1(\frac{\omega_b}{\omega_1})^2 \tag{3.29}$$

$$\bar{L}_3 \approx \frac{P_2}{(1-P_1)^2}(\frac{\omega_b}{\omega_2})^2 \tag{3.30}$$

The orders of $\bar{L}_1$, $\bar{L}_2$ and $\bar{L}_3$ are ϵ^0, ϵ^1 and ϵ^2 respectively, so that there will be a large contribution to the rigid body mode from the earthquake input motion and its contribution to the modes having superstructural deformation are minor. Since the rigid body mode creates little stress in the superstructure, in the base isolation approach there is no need to design the superstructure to resist the earthquake loading and this will thus reduce the cost of the superstructure.

3.3 Dynamic Behavior of Light Equipment on Fixed Base Structure

Figure 10 shows an equipment mass m_e with stiffness k_e mounted on the fifth floor of the fixed base structure. The undamped equations of motion for this system are

$$\mathbf{M}\ddot{\mathbf{u}} + \mathbf{K}\mathbf{u} + k_e(u_5-u_e)\,\mathbf{e}_5 = -\mathbf{M}\mathbf{r}\ddot{u}_g \tag{3.31}$$

$$m_e\ddot{u}_e - k_e u_5 + k_e u_e = -m_e\ddot{u}_g \tag{3.32}$$

where $\mathbf{M}$, $\mathbf{K}$, $\mathbf{r}$ and $\mathbf{u}$ have been defined in Eq. (3.2) to (3.5) and

$$\mathbf{e}_5 = [0\ 0\ 0\ 0\ 1]^T \tag{3.33}$$

where $P_1=R_1L_1^2$ and $P_2=R_2L_2^2$. The generalized mode shapes with respect to these three frequencies are

$$\begin{Bmatrix} \bar{u}_b^{(1)} \\ \bar{Y}_1^{(1)} \\ \bar{Y}_2^{(1)} \end{Bmatrix} \approx \begin{Bmatrix} 1 \\ L_1(\frac{\omega_b}{\omega_1})^2 \\ L_2(\frac{\omega_b}{\omega_2})^2 \end{Bmatrix} \tag{3.25}$$

$$\begin{Bmatrix} \bar{u}_b^{(2)} \\ \bar{Y}_1^{(2)} \\ \bar{Y}_2^{(2)} \end{Bmatrix} \approx \begin{Bmatrix} 1 \\ -\frac{L_1}{P_1}\left[1-(1-P_1)(\frac{\omega_b}{\omega_1})^2+\frac{P_2}{1-P_1}(\frac{\omega_1}{\omega_2})^2\right] \\ \frac{L_2}{1-P_1}(\frac{\omega_1}{\omega_2})^2 \end{Bmatrix} \tag{3.26}$$

$$\begin{Bmatrix} \bar{u}_b^{(3)} \\ \bar{Y}_1^{(3)} \\ \bar{Y}_2^{(3)} \end{Bmatrix} \approx \begin{Bmatrix} 1 \\ -L_1\left[1+\frac{1-P_1-P_2}{1-P_1}(\frac{\omega_1}{\omega_2})^2\right] \\ -\frac{(1-P_1)L_2}{P_2}\left[1-\frac{P_1(1-P_1-P_2)}{(1-P_1)^2}(\frac{\omega_1}{\omega_2})^2\right] \end{Bmatrix} \tag{3.27}$$

The above equations for frequencies and mode shapes illustrate the dynamic behavior of a base-isolated structure. In Eq. (3.25), the component $\bar{Y}_1^{(1)}$ is of the same order as ϵ and $\bar{Y}_2^{(1)}$ is of order ϵ^2. They are much less than the component $\bar{u}_b^{(1)}$, which is of order ϵ^0. The first mode of the base-isolated structure is almost entirely a rigid body mode, in which there is no deformation in the superstructure. The first mode frequency is nearly equal to the natural frequency of a single degree-of-freedom system with the total structural mass as its mass and the stiffness of isolation system as its spring constant. The component $\bar{Y}_2^{(2)}$ in Eq. (3.26), which is of order ϵ, is much less than the other two components. Hence, the second mode of the base-isolated structure is almost entirely the combination of the rigid body mode and the first superstructural mode. Since the third mode frequency and its generalized mode shape in Eq. (3.24) and (3.27) do not have the ω_b term, the third mode of the base-isolated structure is almost independent of the isolation system. In other words, the influence of the isolation system becomes minor and

$$\begin{Bmatrix} \hat{Y}_1^{(2)} \\ \hat{u}_e^{(2)} \end{Bmatrix} \approx \begin{Bmatrix} 1 \\ \frac{1}{2} - \frac{1}{\sqrt{\gamma}} \end{Bmatrix} \tag{3.40}$$

The respective participation factors based on Eq. (3.35) are

$$\hat{L}_1 \approx \frac{L_1}{2} + \frac{2-L_1}{4}\sqrt{\gamma} \tag{3.41}$$

$$\hat{L}_2 \approx \frac{L_1}{2} - \frac{2-L_1}{4}\sqrt{\gamma} \tag{3.42}$$

From the above results, it is easy to show that the first mode of the original structure is split into two modes when the tuned light equipment is included. One mode has a frequency slightly lower than that of the original mode; and the other has a slightly higher frequency. These two mode shapes are plotted on Figure 11. The tuned equipment has a large displacement in each of these modes.

The mode superposition method

$$\begin{Bmatrix} Y_1 \\ u_e \end{Bmatrix} = \hat{Z}_1 \begin{Bmatrix} \hat{Y}_1^{(1)} \\ \hat{u}_e^{(1)} \end{Bmatrix} + \hat{Z}_2 \begin{Bmatrix} \hat{Y}_1^{(2)} \\ \hat{u}_e^{(2)} \end{Bmatrix} \tag{3.43}$$

can be applied to decouple Eq. (3.35). If each mode i is assumed to have a damping ratio $\hat{\xi}_i$, the decoupled equations of motion become

$$\ddot{\hat{Z}}_i + 2\hat{\xi}_i\hat{\omega}_i\dot{\hat{Z}}_i + \hat{\omega}_i^2\hat{Z}_i = -\hat{L}_i\ddot{u}_g \qquad \text{for } i=1,2 \tag{3.44}$$

If the input ground motion is harmonic, $\ddot{u}_g = A_g e^{i\omega t}$ in which A_g is the amplitude, the solution of Eq. (3.44) becomes

$$\hat{Z}_i = \frac{-\hat{L}_i A_g}{\hat{\omega}_i^2 - \omega^2 + 2i\hat{\xi}_i\hat{\omega}_i\omega} e^{i\omega t} \qquad \text{for } i=1,2 \tag{3.45}$$

and the absolute equipment acceleration,

$$\hat{a}_e = \ddot{u}_g + \hat{u}_e^{(1)}\ddot{\hat{Z}}_1 + \hat{u}_e^{(2)}\ddot{\hat{Z}}_2 \tag{3.46}$$

Like Eq. (3.19), the structural displacements are approximated as $\mathbf{u} \approx Y_1 \boldsymbol{\phi}_1$, in which the contribution of higher structural modes has been neglected. Set the first structural mode shape to be

$$\boldsymbol{\phi}_1 = [\phi_1^{(1)} \; \phi_2^{(1)} \; \phi_3^{(1)} \; \phi_4^{(1)} \; 1]^T \tag{3.34}$$

in which the fifth component is unit, so that $u_5 = Y_1$. Then, multiplying $\boldsymbol{\phi}_1^T$ to Eq. (3.31) and applying the properties in Eq. (3.9) to (3.11), the undamped equations of motion become

$$\begin{bmatrix} M_1 & 0 \\ 0 & m_e \end{bmatrix} \begin{Bmatrix} \ddot{Y}_1 \\ \ddot{u}_e \end{Bmatrix} + \begin{bmatrix} M_1\omega_1^2 + k_e & -k_e \\ -k_e & k_e \end{bmatrix} \begin{Bmatrix} Y_1 \\ u_e \end{Bmatrix} = -\begin{Bmatrix} M_1 L_1 \\ m_e \end{Bmatrix} \ddot{u}_g \tag{3.35}$$

To find the extreme response of the equipment, the most critical condition is when the natural frequency of equipment, $\omega_e = \sqrt{\frac{k_e}{m_e}}$, is tuned to the first mode frequency of structure; that is, $\omega_e = \omega_1$. For light equipment with a mass which is much less than that of structure, we define the mass ratio $\gamma = \frac{m_e}{M_1} << 1$. For such a system, the modal frequencies $\hat{\omega}_i$ and the generalized mode shapes satisfy the following eigenvalue equation,

$$\begin{bmatrix} (1+\gamma)\omega_1^2 & -\gamma\omega_1^2 \\ -\omega_1^2 & \omega_1^2 \end{bmatrix} \begin{Bmatrix} \hat{Y}_1^{(i)} \\ \hat{u}_e^{(i)} \end{Bmatrix} = \hat{\omega}_i^2 \begin{Bmatrix} \hat{Y}_1^{(i)} \\ \hat{u}_e^{(i)} \end{Bmatrix} \tag{3.36}$$

When the higher order terms in γ are neglected, the frequencies can be found to be approximately

$$\hat{\omega}_1 \approx \omega_1 \left(1 - \frac{1}{2}\sqrt{\gamma} + \frac{1}{8}\gamma\right) \tag{3.37}$$

$$\hat{\omega}_2 \approx \omega_1 \left(1 + \frac{1}{2}\sqrt{\gamma} + \frac{1}{8}\gamma\right) \tag{3.38}$$

and the generalized mode shapes are

$$\begin{Bmatrix} \hat{Y}_1^{(1)} \\ \end{Bmatrix} \approx \begin{bmatrix} 1 \\ \end{bmatrix} \tag{3.39}$$

in which $\hat{S}_{ai}=S_a(\hat{\omega}_i,\hat{\xi}_i)$.

The Complete Quadratic Combination (CQC) method[11,12] has been shown to be a more accurate approach for finding the maximum response by combining the modal maxima for closely spaced modal frequencies than the SRSS method. The CQC method requires that the modal maxima be combined by use of the following equation,

$$f_{e,max} = \left(\sum_i \sum_j f_{e,max}^{(i)} \rho_{ij} f_{e,max}^{(j)}\right)^{1/2} \tag{3.51}$$

where

$$\rho_{ij} = \frac{8\beta^{3/2}(\xi_i\xi_j)^{1/2}(\xi_i+\xi_j\beta)}{(1-\beta^2)^2+4\xi_i\xi_j\beta(1-\beta)^2+4(\xi_i+\xi_j)^2\beta^2} \tag{3.52}$$

with the frequency ratio $\beta=\dfrac{\omega_j}{\omega_i}$ and modal damping ratios ξ_i and ξ_j. The quantity ρ_{ij} has the property that $\rho_{ij}=\rho_{ji}$ and $\rho_{ii}=1$.

For the present case, it can be shown that

$$\hat{\rho}_{12} \approx \frac{2(\hat{\xi}_1+\hat{\xi}_2)(\hat{\xi}_1\hat{\xi}_2)^{1/2}}{\gamma+(\hat{\xi}_1+\hat{\xi}_2)^2} \tag{3.53}$$

The maximum elastic force acting on the tuned equipment can be found from the two modal maxima in Eq. (3.49) and (3.50),

$$\hat{f}_{e,max} \approx \frac{k_e L_1}{2\omega_1^2\sqrt{\gamma}}\left[(\hat{S}_{a1})^2+(\hat{S}_{a2})^2-2\hat{\rho}_{12}\hat{S}_{a1}\hat{S}_{a2}\right]^{1/2} \tag{3.54}$$

If the damping force acting on the equipment is negligible, the internal force will almost equal to the elastic force and the maximum absolute acceleration of tuned equipment becomes

$$\hat{a}_{e,max} \approx \frac{L_1}{2\sqrt{\gamma}}\left[(\hat{S}_{a1})^2+(\hat{S}_{a2})^2-2\hat{\rho}_{12}\hat{S}_{a1}\hat{S}_{a2}\right]^{1/2} \tag{3.55}$$

Since it is of order $\gamma^{-1/2}$, the acceleration of tuned light equipment in the fixed base structure will be very large.

will also be harmonic. Let $\hat{a}_e=\hat{A}_e e^{i\omega t}$. The ratio of $\frac{|\hat{A}_e|}{A_g}$, called as amplification factor, will be the function of L_1, γ, $\hat{\xi}_i$ and frequency ratio $\frac{\omega}{\omega_1}$. Figure 12 shows the curve of amplification factor versus frequency ratio for the case of $L_1=1.3$, $\gamma=0.0027$ and $\hat{\xi}_1=\hat{\xi}_2=1\%$. This curve shows that the first mode frequency of original structure is split into twin peaks when tuned light equipment is included. Since the frequencies of the twin peaks are very close, the time history of the equipment response when subjected to earthquake excitation will produce a beat phenomenon. Figure 13 displays the acceleration response of tuned equipment for the same case as Figure 12 but with $\omega_1=3.2$Hz and under the El Centro 1940 earthquake input. The characteristics of beat and twin peaks for tuned equipment has been reported by Kelly and Sackman.[9,10] These phenomena result from the interaction of structure and equipment. More complicated models have been analyzed in their reports.

Since the choice of ϕ_1 components, defined in Eq. (3.34), makes $u_5=Y_1$, the elastic force acting on the equipment becomes $f_e=k_e(u_e-Y_1)$. The elastic force contributed by the i'th mode of this base-fixed system is defined as

$$\hat{f}_e^{(i)} = k_e(\hat{u}_e^{(i)}-\hat{Y}_1^{(i)})\hat{Z}_i \tag{3.47}$$

If $S_a(\omega,\xi)$ is the acceleration response spectrum of the input acceleration $\ddot{u}_g$, the maximum response of $\hat{Z}_i$ will be

$$\hat{Z}_{i,max} = \frac{\hat{L}_i}{\hat{\omega}_i^2} S_a(\hat{\omega}_i,\hat{\xi}_i) \quad \text{for } i=1,2 \tag{3.48}$$

It follows that the maximum response of each mode can be found approximately as

$$\hat{f}_{e,max}^{(1)} \approx \frac{L_1}{2\sqrt{\gamma}}\left(1+\frac{\sqrt{\gamma}}{L_1}\right)\frac{k_e}{\omega_1^2}\hat{S}_{a1} \tag{3.49}$$

$$\hat{f}_{e,max}^{(2)} \approx -\frac{L_1}{2\sqrt{\gamma}}\left(1-\frac{\sqrt{\gamma}}{L_1}\right)\frac{k_e}{\omega_1^2}\hat{S}_{a2} \tag{3.50}$$

For the light equipment, the mass ratio, $\gamma=\frac{m_e}{M_1}$, is much less than unity and assumed to have the same order of ϵ^2. The modal frequencies can be found approximately by neglecting the higher order terms of γ and ϵ,

$$\tilde{\omega}_1 \approx \omega_b \tag{3.61}$$

$$\tilde{\omega}_2 \approx \frac{1}{\sqrt{1-P_1}}\omega_1\left(1+\frac{P_1}{4}\epsilon-\frac{1}{2}\delta\right) \tag{3.62}$$

$$\tilde{\omega}_3 \approx \frac{1}{\sqrt{1-P_1}}\omega_1\left(1+\frac{P_1}{4}\epsilon+\frac{1}{2}\delta\right) \tag{3.63}$$

where $\delta=\left[(1-\frac{P_1}{L_1})^2\frac{\gamma}{1-P_1}+(\frac{P_1}{2}\epsilon)^2\right]^{1/2}$, which is of order ϵ. The generalized mode shapes are as following,

$$\begin{Bmatrix}\tilde{u}_b^{(1)}\\ \tilde{Y}_1^{(1)}\\ \tilde{u}_e^{(1)}\end{Bmatrix} \approx \begin{Bmatrix}1\\ L_1\epsilon\\ (1+L_1-P_1)\epsilon\end{Bmatrix} \tag{3.64}$$

$$\begin{Bmatrix}\tilde{u}_b^{(2)}\\ \tilde{Y}_1^{(2)}\\ \tilde{u}_e^{(2)}\end{Bmatrix} \approx \begin{Bmatrix}1\\ -\frac{L_1}{P_1}\left(1-\frac{(1-P_1)(2L_1-P_1)}{2(L_1-P_1)}\epsilon-\frac{(1-P_1)}{(L_1-P_1)}\delta\right)\\ \frac{2(L_1-P_1)}{P_1(P_1\epsilon-2\delta)}\end{Bmatrix} \tag{3.65}$$

$$\begin{Bmatrix}\tilde{u}_b^{(3)}\\ \tilde{Y}_1^{(3)}\\ \tilde{u}_e^{(3)}\end{Bmatrix} \approx \begin{Bmatrix}1\\ -\frac{L_1}{P_1}\left(1-\frac{(1-P_1)(2L_1-P_1)}{2(L_1-P_1)}\epsilon+\frac{(1-P_1)}{(L_1-P_1)}\delta\right)\\ \frac{2(L_1-P_1)}{P_1(P_1\epsilon+2\delta)}\end{Bmatrix} \tag{3.66}$$

and the participation factors become

$$\tilde{L}_1 \approx 1-P_1\epsilon \tag{3.67}$$

$$\tilde{L}_2 \approx \frac{P_1}{2}\epsilon\left(1-\frac{P_1}{2}\frac{\epsilon}{\delta}\right) \tag{3.68}$$

3.4 Dynamic Behavior of Light Equipment on Base-Isolated Structure

When the light equipment is mounted on the base-isolated structure as shown in Figure 14, the undamped equations of motion become

$$m_t\ddot{u}_b + (\mathbf{Mr})^T\ddot{\mathbf{u}} + m_e\ddot{u}_e + k_b u_b = -m_t\ddot{u}_g \tag{3.56}$$

$$\mathbf{Mr}\ddot{u}_b + \mathbf{M}\ddot{\mathbf{u}} + \mathbf{Ku} + k_e(u_5 - u_e)\mathbf{e}_5 = -\mathbf{Mr}\ddot{u}_g \tag{3.57}$$

$$m_e(\ddot{u}_b + \ddot{u}_e) + k_e(u_e - u_5) = -m_e\ddot{u}_g \tag{3.58}$$

where u_e is the equipment displacement relative to the base; m_t is the total mass of entire system, equal to $m_b+m_1+m_2+m_3+m_4+m_5+m_e$; $\mathbf{M}$, $\mathbf{K}$, $\mathbf{r}$ and $\mathbf{u}$ have been defined in Eq. (3.2) to (3.5) and $\mathbf{e}_5$ defined in Eq. (3.33).

As in the derivation in the last section, the superstructure deformation is approximated as $\mathbf{u} \approx Y_1\boldsymbol{\phi}_1$, in which $\boldsymbol{\phi}_1$ is chosen to be the same as Eq. (3.34) so that $u_5 = Y_1$. By multiplying Eq. (3.57) by $\boldsymbol{\phi}_1^T$ and applying the properties in Eq. (3.9) to (3.11), the equations of motion can be reduced to be

$$\begin{bmatrix} m_t & M_1L_1 & m_e \\ M_1L_1 & M_1 & 0 \\ m_e & 0 & m_e \end{bmatrix}\begin{Bmatrix} \ddot{u}_b \\ \ddot{Y}_1 \\ \ddot{u}_e \end{Bmatrix} + \begin{bmatrix} k_b & 0 & 0 \\ 0 & M_1\omega_1^2+k_e & -k_e \\ 0 & -k_e & k_e \end{bmatrix}\begin{Bmatrix} u_b \\ Y_1 \\ u_e \end{Bmatrix} = -\begin{Bmatrix} m_t \\ M_1L_1 \\ m_e \end{Bmatrix}\ddot{u}_g \tag{3.59}$$

In general, the natural frequency of light equipment is much higher than the frequency of rigid body mode. To find the critical response of equipment, the natural frequency of equipment, $\omega_e = \sqrt{\dfrac{k_e}{m_e}}$, is tuned to be equal to $\dfrac{\omega_1}{\sqrt{1-P_1}}$, which is the second mode frequency of the base-isolated structure as shown in Eq. (3.23). For such a base-isolated structure with tuned equipment, the modal frequencies $\tilde{\omega}_i$ and generalized mode shapes can be derived from the following eigenvalue equation

$$\begin{bmatrix} \omega_b^2 & 0 & 0 \\ 0 & (1+\dfrac{\gamma}{1-P_1})\omega_1^2 & -\dfrac{\gamma}{1-P_1}\omega_1^2 \\ 0 & -\dfrac{1}{1-P_1}\omega_1^2 & \dfrac{1}{1-P_1}\omega_1^2 \end{bmatrix}\begin{Bmatrix} \tilde{u}_b^{(i)} \\ \tilde{Y}_1^{(i)} \\ \tilde{u}_e^{(i)} \end{Bmatrix} = \tilde{\omega}_i^2\begin{bmatrix} 1+R_1\gamma & R_1L_1 & R_1\gamma \\ L_1 & 1 & 0 \\ 1 & 0 & 1 \end{bmatrix}\begin{Bmatrix} \tilde{u}_b^{(i)} \\ \tilde{Y}_1^{(i)} \\ \tilde{u}_e^{(i)} \end{Bmatrix} \tag{3.60}$$

case, the second mode frequency of the original base-isolated structure is about $1.8\omega_1$. Twin peaks occur near this frequency. There is an additional peak near $0.19\omega_1$, which corresponds to the frequency of rigid body mode. When the input ground motion is a general earthquake input, the acceleration time history of the tuned equipment will be similar to Figure 17, which has the same condition of the case in Figure 16 but with ω_1=3.2Hz and under El Centro record excitation. Since there is a great deal of contribution from the rigid body mode to the response of the tuned equipment, the beat phenomenon is not obvious in the time history of the equipment response.

The maximum solution of Eq. (3.71) can be found from the acceleration response spectrum of input excitation, $S_a(\tilde{\omega}_i,\tilde{\xi}_i)$,

$$\tilde{Z}_{i,max} = \frac{\tilde{L}_i}{\tilde{\omega}_i^2} S_a(\tilde{\omega}_i,\tilde{\xi}_i) \qquad \text{for } i=1,2,3 \tag{3.74}$$

Like Eq. (3.47), the maximum contribution of each mode to the elastic force acting on equipment will be

$$\tilde{f}_{e,max}^{(1)} \approx \frac{k_e(1-P_1)}{\omega_1^2}\tilde{S}_{a1} \tag{3.75}$$

$$\tilde{f}_{e,max}^{(2)} \approx -\frac{(L_1-P_1)\epsilon}{2\delta}\frac{k_e(1-P_1)}{\omega_1^2}\tilde{S}_{a2} \tag{3.76}$$

$$\tilde{f}_{e,max}^{(3)} \approx \frac{(L_1-P_1)\epsilon}{2\delta}\frac{k_e(1-P_1)}{\omega_1^2}\tilde{S}_{a3} \tag{3.77}$$

in which $\tilde{S}_{ai}=S_a(\tilde{\omega}_i,\tilde{\xi}_i)$.

By the CQC method defined in Eq. (3.51) and (3.52), the maximum elastic force on the tuned equipment can be found as

$$\tilde{f}_{e,max} \approx \left[(\tilde{f}_{e,max}^{(1)})^2 + (\tilde{f}_{e,max}^{(2)})^2 + (\tilde{f}_{e,max}^{(3)})^2 + 2\tilde{\rho}_{23}\tilde{f}_{e,max}^{(2)}\tilde{f}_{e,max}^{(3)} \right]^{1/2} \tag{3.78}$$

in which the terms of $\tilde{\rho}_{12}$ and $\tilde{\rho}_{13}$ which are of order $\epsilon^{3/4}$ have been neglected and

$$\tilde{\rho}_{23} \approx \frac{2(\tilde{\xi}_2+\tilde{\xi}_3)(\tilde{\xi}_2\tilde{\xi}_3)^{1/2}}{\delta^2+(\tilde{\xi}_2+\tilde{\xi}_3)^2} \tag{3.79}$$

$$\tilde{L}_3 \approx \frac{P_1}{2}\epsilon\left(1+\frac{P_1}{2}\frac{\epsilon}{\delta}\right) \tag{3.69}$$

As in the case of the fixed base structure, the original second mode of the isolated structure is split into two modes when the tuned equipment is mounted. The first three mode shapes are shown in Figure 15. The first mode is still a rigid body mode. The tuned equipment has a large displacement in the second and third mode shapes, which is of the order ϵ^{-1}. However, the participation factors of these two modes are of order ϵ and the equipment response on this base-isolated structure will not be very large.

Eq. (3.59) can be decoupled by using mode superposition

$$\begin{Bmatrix} u_b \\ Y_1 \\ u_e \end{Bmatrix} = \tilde{Z}_1 \begin{Bmatrix} \tilde{u}_b^{(1)} \\ \tilde{Y}_1^{(1)} \\ \tilde{u}_e^{(1)} \end{Bmatrix} + \tilde{Z}_2 \begin{Bmatrix} \tilde{u}_b^{(2)} \\ \tilde{Y}_1^{(2)} \\ \tilde{u}_e^{(2)} \end{Bmatrix} + \tilde{Z}_3 \begin{Bmatrix} \tilde{u}_b^{(3)} \\ \tilde{Y}_1^{(3)} \\ \tilde{u}_e^{(3)} \end{Bmatrix} \tag{3.70}$$

If each mode i is assumed to have a damping ratio $\tilde{\xi}_i$, the decoupled equations of motion will be

$$\ddot{\tilde{Z}}_i + 2\tilde{\xi}_i\dot{\tilde{Z}}_i + \tilde{\omega}_i^2\tilde{Z}_i = -\tilde{L}_i\ddot{u}_g \quad \text{for } i=1,2,3 \tag{3.71}$$

When the ground motion is harmonic, $\ddot{u}_g = A_g e^{i\omega t}$, the solution of Eq. (3.71) becomes

$$\tilde{Z}_i = \frac{-\tilde{L}_i A_g}{\tilde{\omega}_i^2 - \omega^2 + 2i\tilde{\xi}_i\tilde{\omega}_i\omega} e^{i\omega t} \quad \text{for } i=1,2,3 \tag{3.72}$$

The absolute equipment acceleration, which is the summation of ground motion and mode components as follows

$$\tilde{a}_e = \ddot{u}_g + (\tilde{u}_b^{(1)}+\tilde{u}_e^{(1)})\ddot{\tilde{Z}}_1 + (\tilde{u}_b^{(2)}+\tilde{u}_e^{(2)})\ddot{\tilde{Z}}_2 + (\tilde{u}_b^{(3)}+\tilde{u}_e^{(3)})\ddot{\tilde{Z}}_3 \tag{3.73}$$

is also harmonic, $\tilde{a}_e = \tilde{A}_e e^{i\omega t}$. The amplification factor $\frac{|\tilde{A}_e|}{A_g}$ will be the function of L_1, P_1, γ, ϵ, $\tilde{\xi}_i$ and frequency ratio $\frac{\omega}{\omega_1}$. Figure 16 shows the curve of amplification factor versus frequency ratio for the case of $L_1=1.3$, $P_1=0.69$, $\gamma=0.0015$, $\epsilon=0.035$, $\tilde{\xi}_1=6\%$, and $\tilde{\xi}_2=\tilde{\xi}_3=1\%$. In this

Chapter 4 EXPERIMENTAL PROGRAM AND RESULTS

4.1 Five-Story Frame Structural Model

The experimental model used is shown in Figure 18. It is a five-story steel frame mounted on two heavy base floor girders that are supported by four rubber bearings resting on load cells. The load cells are anchored to the shaking table with high-tension stress rods. The model can be considered as a section through the weak direction of a typical frame structure at a scale factor of approximately one third. The dead load provided by concrete blocks, which are tied down to the frame at various floor levels, is 12 kips at each level. The total weight of the entire structure is about 80 kips, including the weight of frame. Thus, a compressive force of approximately 20 kips is produced in each bearing. The dead load provided by the concrete blocks produces stress levels comparable to those in a full structural frame.

4.2 Elastomeric Bearings and Foundation Systems

The elastomeric bearings for the base isolation test, as shown in Figure 19, are of polychloroprene rubber reinforced by steel plates. A cylindrical bearing design is used so as to minimize the formation of localized stress concentration. A hole is provided in the center of the bearing to facilitate the insertion of the lead plug. The dimensions of each bearing are as follows: an outside diameter of 5.5 inches and an inside diameter of 2.0 inches; a total height of 5.5 inches; an effective elastomer height of 2.5 inches; 44 layers of elastomer, each layer approximately 0.057 inch thick; 43 layers of steel plate, each layer approximately 0.06 inch thick; and two end plates 7 inches by 7 inches square and 0.250 inch thick.

There were three different foundation systems in the test series, namely:

(1) fixed base.

(2) base isolated by elastomeric bearing without lead plug (no-lead bearing).

(3) base isolated by elastomeric bearing with lead plug (lead bearing).

Using Eq. (3.75) to Eq. (3.77), the maximum elastic force becomes

$$\tilde{f}_{e,max} \approx \frac{k_e(1-P_1)}{\omega_1^2}\left|(\tilde{S}_{a1})^2+\frac{(L_1-P_1)^2\epsilon^2}{4\delta^2}((\tilde{S}_{a2})^2+(\tilde{S}_{a3})^2-2\tilde{\rho}_{23}\tilde{S}_{a2}\tilde{S}_{a3})\right|^{1/2} \tag{3.80}$$

If the damping force acting on the equipment is very small, its inertial force will about equal to the elastic force and the maximum absolute acceleration of tuned equipment becomes

$$\tilde{a}_{e,max} \approx \left|(\tilde{S}_{a1})^2+\frac{(L_1-P_1)^2\epsilon^2}{4\delta^2}((\tilde{S}_{a2})^2+(\tilde{S}_{a3})^2-2\tilde{\rho}_{23}\tilde{S}_{a2}\tilde{S}_{a3})\right|^{1/2} \tag{3.81}$$

It is of order γ^0. The isolation effect is obvious when comparing with the maximum acceleration of the tuned equipment on the fixed base system in Eq. (3.55), which is of order $\gamma^{-1/2}$.

Although the derivation in this chapter assumes that the light equipment is mounted on the fifth floor, the results apply to those cases where the equipment is mounted on any other floor. The only change is that ϕ_1, defined in Eq. (3.34), should be reset to have its i'th component unit if the equipment is mounted on the i'th floor. Also, the corresponded values M_1, L_1, R_1 and P_1 will be changed. Since the basic equations remain the same, the behavior of the tuned equipment will be the same as that discussed in this chapter even though it is mounted on the other floor.

full-scale structure to the historical earthquakes and the displacements in the model will correspond to one third of those for the full-scale structure.

The four earthquake records used are the El Centro 1940 S00E component, the Taft 1952 S69E component, the Parkfield 1966 N65E component, and the Pacoima Dam 1971 S14W component. The El Centro and Taft records are typical California earthquake records, one representing a long duration record and the other a short duration signal with dominant frequencies in the 1 Hz to 5 Hz range. The Parkfield record is a short duration signal with considerable low-frequency energy in the region below 1 Hz. Since the fundamental frequency of the base-isolated structure is located in this region, this input is an extremely severe test for the isolation system. The Pacoima Dam record has frequencies in a slightly higher range but has a high-frequency pulse in the middle of the signal that produces a very high acceleration. The normalized acceleration time histories of the four records, and their Fourier spectra, are shown in Figure 20 and Figure 21.

The shaking table is a 20 ft x 20 ft x 1 ft prestressed concrete slab, driven independently in the vertical direction and one horizontal direction by servo-controlled actuators. The control signals for the motion in these two directions are in the form of analog displacement time histories. The maximum table displacement and acceleration produced by the shaking table can be varied by the span setting, which is directly related to the maximum table displacement. In this shaking table system, a peak table displacement of ± 5 in, which is the limit of table motion, is arbitrarily given a span setting of 1000. Lower span numbers correspond to proportionally lower peak displacements.

4.5 Extreme Values of Oscillator Response

The individual values of peak acceleration for the three oscillators and the fifth floor to which they are attached are tabulated in Table 1 for each of the three foundation conditions and the four input signals with only horizontal input to the shake table.

In the case of the lead bearing system, only two of the four bearings were filled. Since the table motion is in one horizontal direction, no complication arises if two are filled and two are not. The lead plug inserted in the central hole of the bearing is a cylinder with a diameter of 2.0 inches and a height of 5.5 inches. The yield stress of lead is 1.4 kip/in^2. Thus, in the lead bearing system, the volume ratio of lead to elastomer is one sixth and the nominal yield base shear is approximately 9 kips which is 11 per cent of the total weight of the model.

4.3 Oscillators to Simulate Light Equipment

Three oscillators were used in this test to simulate light equipment. The oscillators were attached to the concrete blocks of the structural model at the fifth floor as shown in Figure 18. They were very simple vertical cantilevers with an added weight to which an accelerometer is attached. The oscillator 1 was adjusted to have its fixed base natural frequency close to the frequency of the lowest mode of the fixed base structural model. It was designed using a double cantilever beam with four 20-lb weights and it was tuned to the frequency of 3.2 Hz. The oscillator 2 was tuned to the second mode frequency of the base-isolated structure. It was a single cantilever beam carrying two 20-lb weights with the natural frequency of 5.5 Hz. The oscillator 3 was tuned to the third mode frequency of the base-isolated structure. It was a single cantilever beam, carrying one 20-lb weight, having the natural frequency of 15.2 Hz. The second and third oscillators were tuned to the two lowest structural modes of the isolated structure. The rigid body isolated mode was neglected for the reason that it is highly unlikely that an item of light equipment would have such a low frequency.

4.4 Earthquake Input Signals and Shaking Table Test

Four earthquake input signals, based on records of historical California earthquakes, were used for this test series. Each was run in time scaled at a factor of $\sqrt{3}$. This time scaling of the earthquake inputs corresponds to the geometrical scale of the model; in this scaling the acceleration response of the model to these inputs will correspond to the actual acceleration of a

system, are calculated from Table 1 and summarized in Table 3. The mean values of reduction factor for the system isolated by plain bearings is over 10. The reduction effect on peak oscillator acceleration is much larger than that for the system with lead bearings. Although the lead bearings can reduce the relative displacement between the structure and the ground, its effect on the reduction of the acceleration of the oscillators is not great. It seems probable however that the amount of lead used in the bearings for this experiment is rather more than required under optimum conditions. The presence of the lead increases the stiffness of the bearings and by increasing the effective isolation frequency has a tendency to reduce the degree of isolation of the system.

4.6 Influence of Vertical Excitation

The peak accelerations of the response to the three earthquake signals with combined horizontal and vertical input are summarized in Table 4. No vertical signal is available for the Parkfield record. The magnification ratios and reduction factors for the two kinds of base-isolated system are calculated from Table 4 and illustrated in Table 5. On the system isolated by the no-lead bearing, the magnification factors of oscillators 2 and 3 are much larger than those under horizontal only input; and their reduction factors are much smaller.

The use of only four bearings to support the structural model which had eight columns means that the columns and bearings are not lined up and thus the base girders carry large bending moments which would not appear if eight bearings were used. These bending moments in the base girders are particularly severe when vertical accelerations are included in the input. They cause spurious horizontal accelerations in the frame even when vertical input only is applied and distort the horizontal accelerations when both horizontal and vertical motions are applied simultaneously. This phenomenon has been discussed in a previous report.[6] When bearings are directly under the columns the horizontal acceleration due to vertical input are negligible.[13,14]

The ratios of the peak acceleration of oscillators and the fifth floor to that of the shaking table input, referred to as the magnification ratio, are calculated from Table 1 and listed in Table 2. The mean values of the magnification ratios for the four input signals show clearly that the ratios for the base-isolated systems are smaller than those for the base-fixed system, even when the oscillators are tuned to the modal frequencies of the base-isolated structure. In the case of the structure with no-lead bearings, the magnification ratios are all less than one. This means the peak accelerations of the oscillators are smaller than those of the input signals. This attenuation effect will always take place when the bearing is soft enough to lower the first mode frequency of the base-isolated structure well below the dominant earthquake frequencies and has been shown analytically in the last chapter.

As stated before that the Parkfield record is a severe input for the base-isolated system, the magnification ratios of the fifth floor acceleration under the Parkfield record is 0.299 for the system without lead and 0.958 for the system with lead plugs. These ratios are larger than those for the other three records. In contrast, the magnification ratio for the Parkfield signal is 2.599 for the fixed base system which is the smallest value of the four input records.

Since the oscillator 1 was tuned to the first mode frequency of the base-fixed structure, its magnification ratio is higher than the other two oscillators on the fixed base system. Similarly, due to tuning to the modal frequencies of the base-isolated structures, the magnification ratios of oscillators 2 and 3 are larger than that for oscillator 1 on the two base-isolated systems.

To demonstrate the nonlinear response of the lead bearing system, the model was subjected to a series of El Centro input motions with steadily increasing span, corresponding to increasing intensity from a peak acceleration of 0.115g to one of 1.463g. The magnification ratios of oscillators and the fifth floor with respect to different horizontal spans are plotted on Figure 22. There is a clear trend for the magnification ratios to decrease with increasing span, so that the isolation effect of the lead bearing system increases with increased input intensity.

To compare the efficiency of different isolation systems, reduction factors, defined as the ratio of the oscillator peak acceleration for the base-isolated system to that for the fixed base

characters but the beat phenomenon is clearer. As shown on the Fourier spectra of Figure 26 and 32, the amplitudes at the peak frequency for the three oscillators on this base-isolated system are much smaller than those on the fixed base system. This shows that the energy introduced into the oscillators on the isolation system is significantly less than in the fixed base case.

For the system isolated by the lead bearing system, the first three mode frequencies are approximately 1.4 Hz, 6.7 Hz, 14.8 Hz. Due to the nonlinear behavior of the lead bearings, a sharp peak does not appear at the first mode frequency in the Fourier spectra of frame response as shown in Figure 27 and 33. Unlike the no-lead bearing case, all three oscillators do not have a concentrated frequency content near the frequency of the first mode, as shown in Figure 28 and 34. There is a larger shift in the second mode frequency than that in the no-lead bearing case from the first mode frequency of the fixed base system, and this leads to oscillator 2 not being tuned. In the third mode, the influence of the isolation system is less and the superstructure behavior becomes dominant, as derived in the previous chapter. Thus, the third mode frequencies are almost the same for both the lead bearing case and the no-lead bearing case. The oscillator 3 in the lead bearing case shows both beat and double peak phenomena. Since the lead plug acts as an energy dissipator, decay is shown in the time histories of oscillator response. As shown on the Fourier spectra of Figure 28 and 34, the amplitudes of peak frequency for the three oscillators on this base-isolated system are slightly smaller than those on the fixed base system and much larger than those on the system isolated by the no-lead bearing. In other words, the lead-rubber bearing isolation system used in these experiments is not very efficient in reducing the energy transmitted from the table into the superstructure.

4.7 Time Histories and Fourier Spectra of Oscillator Response

In order to show the differences in behavior among the three kinds of base conditions, the acceleration time histories and Fourier spectra for the response of the frames and oscillators are shown in Figure 23 through Figure 34 under the El Centro and Parkfield records with horizontal only input. The Fourier spectrum of structural acceleration response can show the distribution of the energy introduced into the structure at different frequencies. The amplitude in a Fourier spectrum can indicate relative amounts of energy at different frequencies if the duration and time intervals used for each record are the same. In order to compare the response of the frame and oscillators for the three foundation systems, the duration of all time histories used in the Fast Fourier Transform are set to be 20.48 seconds with an interval of 0.01 second.

The first mode frequency of the fixed base system was found to be 3.2 Hz. Since the natural frequency of the oscillator 1 is tuned exactly to this value, the beat phenomenon is very clear in the acceleration time history of oscillator 1 on the fixed base system, as shown in Figure 24 and 30. Twin peaks also appear in the Fourier spectrum near its natural frequency. These two characteristics of tuned light equipment have been referred to the last chapter. Although the second and third oscillators are not tuned to the first mode frequency, their Fourier spectra do show that some energy is introduced into these oscillators at this frequency.

The frequencies of the first three modes of the system isolated by the no-lead bearings were measured to be 0.6 Hz, 6.0 Hz, 15.0 Hz. The Fourier spectra of this isolation system, as shown in Figure 25 and 31, reveal that the response of frame has a major frequency content near the first mode frequency. The frequency contents of the response of all three oscillators, as shown in Figure 26 and 32, also has some energy at the first mode frequency, even though they were not tuned to that frequency. Since the oscillator 2 is tuned to the second mode frequency, its Fourier spectra has a double peak near that frequency, but the beat phenomenon is not clear in the time histories, due to the contribution of the first mode frequency to the oscillator response which has been shown in the last chapter. The natural frequency of the oscillator 3 is tuned to the third mode frequency of the isolated system, so that its response has similar

superstructure mode, the modal frequencies and generalized mode shapes have been given in Eq. (3.37) to Eq. (3.40). Like Eq. (5.3), the modal damping ratios can be derived as

$$\hat{\xi}_1 = \hat{\xi}_2 = \frac{\xi_1+\xi_e}{2} \tag{5.7}$$

For the equipment on the base-isolated structure shown in Figure 14, the damped equations of motion can be written as

$$m_t\ddot{u}_b + (\mathbf{Mr})^T\ddot{\mathbf{u}} + m_e\ddot{u}_e + c_b\dot{u}_b + k_b u_b = -m_t\ddot{u}_g \tag{5.8}$$

$$\mathbf{Mr}\ddot{u}_b + \mathbf{M}\ddot{\mathbf{u}} + \mathbf{C}\dot{\mathbf{u}} + c_e(\dot{u}_5-\dot{u}_e)\mathbf{e}_5 + \mathbf{K}\mathbf{u} + k_e(u_5-u_e)\mathbf{e}_5 = -\mathbf{Mr}\ddot{u}_g \tag{5.9}$$

$$m_e\ddot{u}_b + m_e\ddot{u}_e + c_e(\dot{u}_e-\dot{u}_5) + k_e(u_e-u_5) = -m_e\ddot{u}_g \tag{5.10}$$

where c_b is the damping of the bearing. Let $\mathbf{u}\approx Y_1\boldsymbol{\phi}_1$ and multiply $\boldsymbol{\phi}_1^T$ to Eq. (5.9). The damped equations of motion are simplified and similar to Eq. (3.59), except that the following damping force term is added to the left side,

$$\begin{bmatrix} 2\xi_b\omega_b m_f & 0 & 0 \\ 0 & 2\xi_1\omega_1 M_1+2\xi_e\omega_e m_e & -2\xi_e\omega_e m_e \\ 0 & -2\xi_e\omega_e m_e & 2\xi_e\omega_e m_e \end{bmatrix} \begin{Bmatrix} \dot{u}_b \\ \dot{Y}_1 \\ \dot{u}_e \end{Bmatrix} \tag{5.11}$$

where $\xi_b = \frac{c_b}{2\omega_b m_f}$. When the natural frequency of equipment is tuned to the frequency of the second base-isolated mode, the modal frequencies and generalized mode shapes have been given in Eq. (3.61) to Eq. (3.66). Thus, the modal damping ratios can be derived as

$$\tilde{\xi}_1 = \xi_b \tag{5.12}$$

$$\tilde{\xi}_2 = \frac{1}{2}\left[(1-\frac{P_1\epsilon}{2\delta})\frac{\xi_1+P_1\sqrt{\epsilon}\xi_b}{\sqrt{1-P_1}} + (1+\frac{P_1\epsilon}{2\delta})\xi_e \right] \tag{5.13}$$

$$\tilde{\xi}_3 = \frac{1}{2}\left[(1+\frac{P_1\epsilon}{2\delta})\frac{\xi_1+P_1\sqrt{\epsilon}\xi_b}{\sqrt{1-P_1}} + (1-\frac{P_1\epsilon}{2\delta})\xi_e \right] \tag{5.14}$$

Because the first mode is a rigid body mode, only the damping of the bearings contributes to $\tilde{\xi}_1$.

Chapter 5 CORRELATION BETWEEN ANALYSIS AND EXPERIMENT

5.1 Evaluation of Modal Damping Ratios

The damped equation of motion for the fixed base model shown in Figure 8 can be written as

$$\mathbf{M}\ddot{\mathbf{u}} + \mathbf{C}\dot{\mathbf{u}} + \mathbf{K}\mathbf{u} = -\mathbf{M}\mathbf{r}\ddot{u}_g \tag{5.1}$$

where C is the damping matrix of the superstructure. The mode shape, $\boldsymbol{\phi}_i$, is orthogonal with respect to M and K as shown in Eq. (3.7) and in general not orthogonal with respect to C. In order to decouple the damped equation of motion, it is usually assumed that

$$\boldsymbol{\phi}_i^T \mathbf{C} \boldsymbol{\phi}_j = 0 \quad \text{for } i \neq j \tag{5.2}$$

and the damping ratio is defined as

$$\xi_i = \frac{\boldsymbol{\phi}_i^T \mathbf{C} \boldsymbol{\phi}_i}{2\omega_i \boldsymbol{\phi}_i^T \mathbf{M} \boldsymbol{\phi}_i} \tag{5.3}$$

For the equipment on the fixed base structure shown in Figure 10, the damped equations of motion can be written as

$$\mathbf{M}\ddot{\mathbf{u}} + \mathbf{C}\dot{\mathbf{u}} + c_e(\dot{u}_5 - \dot{u}_e)\mathbf{e}_5 + \mathbf{K}\mathbf{u} + k_e(u_5 - u_e)\mathbf{e}_5 = -\mathbf{M}\mathbf{r}\ddot{u}_g \tag{5.4}$$

$$m_e\ddot{u}_e + c_e(\dot{u}_e - \dot{u}_5) + k_e(u_e - u_5) = -m_e\ddot{u}_g \tag{5.5}$$

where c_e is the damping of equipment. Let $\mathbf{u} \approx Y_1\boldsymbol{\phi}_1$ and multiply $\boldsymbol{\phi}_1^T$ to Eq. (5.4). The damped equations of motion are simplified and similar to Eq. (3.35), except that the following damping force term is added to the left side,

$$\begin{bmatrix} 2\xi_1\omega_1 M_1 + 2\xi_e\omega_e m_e & -2\xi_e\omega_e m_e \\ -2\xi_e\omega_e m_e & 2\xi_e\omega_e m_e \end{bmatrix} \begin{Bmatrix} \dot{Y}_1 \\ \dot{u}_e \end{Bmatrix} \tag{5.6}$$

where ξ_1 is the damping ratio of the first superstructure mode defined in Eq. (5.3) and $\xi_e = \frac{c_e}{2\omega_e m_e}$. When the natural frequency of equipment is tuned to the frequency of the first

The damping of the steel frame used in the experiment is small if the deformation is in the elastic range. It is reasonable to assume that the damping ratio of the first superstructural mode, ξ_1, is equal to 2.0%. Compared with the damping in the steel frame, the damping of oscillators, ξ_e, is negligible. Thus, by Eq. (5.7), $\hat{\xi}_1=\hat{\xi}_2=1.0\%$. From Figure 35, $N_a(3.2Hz,1.0\%)$ is found to be 2.76 and the magnification ratio, calculated from Eq. (5.17), is 45.1. This value is much higher than the mean value of the experiment results, 8.016, as shown in Table 2.

The main reason for this inconsistency is that the base was not completely fixed in the experiment. As shown in Figure 18, the base girders did not directly rest on the shaking table in the fixed base test. The base girders were bolted to the transverse girders which were mounted on the shaking table. If the base girder had been bolted perfectly, the base would be completely fixed and the magnification ratio of the base would be equal to one. However, the magnification ratio of the base obtained from the experiment, as shown in Table 2, has a mean value of 2.365. This reveals that the base was not completely fixed. To match the mean value of the equipment magnification ratio obtained from the experiment, an equivalent damping ratio of 9% should be introduced into the analysis model. In other words, a great deal of energy is dissipated in the frame due to the incompletely fixed base.

5.3 Response of Base-Isolated System

The weight of base in the experiment model is about 15 kips and the total frame weight becomes 80 kips. Thus

$$R_1 = \frac{M_1}{m_f} = 0.413 \tag{5.18}$$

and

$$P_1 = R_1 L_1^2 = 0.691 \tag{5.19}$$

5.2 Response of Fixed Base System

The mode shape of the superstructure can be obtained from the amplitude, at the respective frequency, of the Fourier spectra of each floor displacement measured for the fixed base system. The mode shape for the first superstructure mode, for which modal frequency is measured as $\omega_1=3.2Hz$, is found to be

$$\phi_1 = [\,0.232 \;\; 0.482 \;\; 0.696 \;\; 0.875 \;\; 1.000\,]^T \tag{5.15}$$

The weight of each floor is about 13 kips. Thus, the modal mass of the first mode, calculated from Eq. (3.9), is $M_1=33.0kip/g$ and the participation factor, calculated from Eq. (3.11), is $L_1=1.294$. The weight of Oscillator 1, which is tuned to 3.2 Hz, is 80 lbs. Including the weight of accelerometer and support, the total weight of the simulated equipment is about 90 lbs. Thus,

$$\gamma = \frac{m_e}{M_1} = 0.00273 \tag{5.16}$$

The magnification ratio of the tuned equipment on the fixed base structure which is defined as $MR=\dfrac{\hat{a}_{e,max}}{\max|\ddot{u}_g|}$ can be derived from Eq. (3.55) by replacing $S_a(\omega,\xi)$ with $N_a(\omega,\xi)$ where $N_a(\omega,\xi)=\dfrac{S_a(\omega,\xi)}{\max|\ddot{u}_g|}$ is the normalized acceleration response spectrum of the ground motion. In order to correlate this with the experimental magnification ratio given in Table 2, normalized acceleration response spectra are obtained from the table input acceleration of the four earthquakes used for the fixed base test. $N_a(\omega,\xi)$, as shown in Figure 35, is the average of these four normalized acceleration response spectra. Since $\hat{\xi}_1=\hat{\xi}_2$ and $\hat{\omega}_1\approx\hat{\omega}_2\approx\omega_1$, Eq. (3.55) can be further simplified as

$$MR \approx \frac{L_1}{\sqrt{2\gamma+8\hat{\xi}_1^2}} N_a(\omega_1,\hat{\xi}_1) \tag{5.17}$$

be

$$\tilde{\xi}_1 = 6.0\% , \quad \tilde{\xi}_2 = 1.6\% , \quad \tilde{\xi}_3 = 3.4\% \tag{5.25}$$

and the value of $\tilde{\rho}_{23}$, obtained from Eq. (3.79), is 0.627

The magnification ratio of the tuned equipment on the base-isolated structure can be derived from Eq (3.81) by replacing $S_a(\omega,\xi)$ with $N_a(\omega,\xi)$. With the values of the variables substituted, it becomes

$$MR = \left[(.181)^2+(.0925)\left[(2.98)^2+(2.39)^2\right]-(.116)(2.98)(2.39)\right]^{1/2} = 0.746 \tag{5.26}$$

where $\tilde{\omega}_2 \approx \tilde{\omega}_3 \approx \bar{\omega}_2 \approx 5.8Hz$ and $N_a(0.6Hz,6.0\%)=0.181$, $N_a(5.8Hz,1.6\%)=2.98$ and $N_a(5.8Hz,3.4\%)=2.39$, which are obtained from Figure 36. This value is a little higher than the mean value obtained from the experiment, 0.645, as shown in Table 2. The experiment result is lower because Oscillator 2 was not precisely tuned on the frequency of the second mode, 6.0 Hz, but was tuned on 5.5 Hz.

The weight of Oscillator 2, which is tuned to 5.5 Hz, is 40 lbs. Including the weight of accelerometer and support, the total weight of this item of equipment is 50 lbs and

$$\gamma = \frac{m_e}{M_1} = 0.00152 \tag{5.20}$$

The frequency of the rigid body mode has been measured in the test of the base-isolated system with the no-lead bearings, ω_b=0.6Hz, and

$$\epsilon = (\frac{\omega_b}{\omega_1})^2 = 0.0352 \tag{5.21}$$

Note that γ is of order ϵ^2, which is an assumption made in Chapter 3, and δ, which is of order ϵ, becomes

$$\delta = \left((1-\frac{P_1}{L_1})^2 \frac{\gamma}{1-P_1} + (\frac{P_1}{2}\epsilon)^2 \right)^{1/2} = 0.0349 \tag{5.22}$$

Using Eq. (3.23), the frequency of the second mode is calculated approximately to be

$$\bar{\omega}_2 \approx \frac{\omega_1}{\sqrt{1-P_1}} = 5.8\ Hz \tag{5.23}$$

This is very close to the measured frequency 6.0 Hz.

For a base-isolated structure, the response is almost entirely in the rigid body mode. The magnification ratio of the base can be approximated as

$$MR = N_a(\omega_b, \xi_b) \tag{5.24}$$

where $N_a(\omega,\xi)$, as shown in Figure 36, is the average of the normalized acceleration response spectra that are computed from the table input accelerations of the four earthquakes used in the test of the base-isolated structure with the no-lead bearings. The magnification ratio of the base obtained from the experiment is 0.179 as shown in Table 2 and $N_a(0.6Hz, 6.0\%)$, obtained from Figure 36, is equal to 0.181. Thus, it can be estimated that ξ_b=6.0%. Assuming that the damping ratio of the first superstructure mode, ξ_1, is 2.0% and ξ_e is negligible, the damping ratios of the base-isolated structure with the tuned equipment are found from Eq. (5.12) to Eq. (5.14) to

The size of these displacements can be reduced by integrating the bearing with an energy-absorbing mechanism such as the lead plug system at the cost of higher equipment forces.

The response of equipment on the no-lead bearing system can be qualitatively described very well by the approximated solution of the elastic models. The theoretical derivation shows that the acceleration response of the tuned equipment on the linear elastic base isolation system is the same order of the magnitude of the corresponding frequency in the acceleration response spectrum of ground input. The results of this theoretical model are well correlated with the experimental results of the no-lead bearing system.

The lead-rubber bearing can dissipate energy through the yielding of the lead. Results using a bilinear model to simulate its force-displacement relation are satisfactory. The experiments have shown that the displacement of the structure relative to the ground was decreased using lead but the equipment accelerations were increased. It seems clear from the results that the amount of lead in the bearing was somewhat greater than optimum. Had it been possible to reduce slightly the amount of lead in the bearing, the accelerations experienced by the equipment might possibly have been reduced and the degree of seismic protection increased while maintaining displacements within safe limits for the bearing. The optimum volume ratio of lead to rubber in the bearing depends on the allowable maximum displacement, the total structural weight and the intensity of earthquake excitation.

Chapter 6 CONCLUSIONS

The mathematical analysis and experimental program have shown that base isolation can produce a very substantial reduction in the seismic response of light internal equipment. In addition, due to the fact that the primary structure above the isolation system moves almost as a rigid body, all support points of a piping system through multiple stories have very nearly the same displacement time history and the effect of multiple support excitation is minimized. All these are considerable implications for the seismic protection of buildings containing important equipment or piping systems. For such a building, the seismic assurance of equipment and piping systems continues to be one of the most expensive and uncertain aspects of building design. The use of an isolation raft for the entire building would reduce the design costs for equipment and piping systems and provide increased protection.

The seismic protection of base isolation depends on shifting the fundamental frequency of the structure out of the range of frequencies which dominate in the earthquake input. Hence, the structural type of the building and the soil conditions at the site might affect the efficiency of the isolation system. For general soil conditions for which earthquakes have dominant frequencies in the range between 1 Hz and 10 Hz, base isolation is applicable to buildings of rigid construction, for example, masonry or reinforced concrete buildings below 14 stories. A building greater than 14 stories will have a fundamental frequency below the dominant range of the earthquake and will in any case be resistant to lateral loads due to wind load requirements. For buildings on very soft soil conditions for which the dominant earthquake frequencies are below 1 Hz, base isolation would not be suitable since it would shift the structural frequency into the more critical range.

Of the systems tested, the isolated system on the bearings without lead provides the greatest protection to the equipment. The equipment accelerations are smaller than the ground acceleration and no amplification of acceleration takes place. However, this advantage is achieved at the cost of increased relative displacements between the structure and the ground.

14. J. M. Kelly and D. E. Chitty, "Control of seismic response of piping systems and components in power plants by base isolation", *Engineering Structures*, **2**, 187-198 (1980).

References

1. J. M. Kelly, "The development of base isolation for the seismic protection of structures", in "Control of seismic response of piping systems and other structure by base isolation" edited by J. M. Kelly, *Report No. UCB/EERC-81/01*, Earthquake Engineering Research Center, University of California, Berkeley (1981).

2. J. M. Kelly, "The influence of base isolation on the seismic response of light secondary equipment", *Report No. UCB/EERC-81/17*, Earthquake Engineering Research Center, University of California, Berkeley (1981).

3. J. M. Kelly, K. E. Beucke and M. S. Skinner, "Experimental testing of a friction damped aseismic base isolation system with fail-safe characteristics", *Report No. UCB/EERC-80/18*, Earthquake Engineering Research Center, University of California, Berkeley (1980).

4. J. M. Kelly, M. S. Skinner and K. E. Beucke, "Experimental testing of an energy-absorbing base isolation system", *Report No. UCB/EERC-80/35*, Earthquake Engineering Research Center, University of California, Berkeley (1980).

5. L. M. Megget, "Analysis and design of a base-isolated reforced concrete frame building", *Bulletin of the New Zealand National Society for Earthquake Engineering*, **11**, 245-254 (1978).

6. J. M. Kelly and S. B. Hodder "Experimental study of lead and elastomeric dampers for base isolation systems", *Report No. UCB/EERC-81/16*, Earthquake Engineering Research Center, University of California, Berkeley (1981).

7. W. H. Robinson, "Lead-rubber hysteretic bearings suitable for protecting structures during earthquakes", *Earthquake Engineering and Structural Dynamics*, **10**, 593-604 (1982).

8. V. Jeng, "Dynamic analysis of base isolation system", *Ph. D. Thesis*, S.E.S.M., Department of Civil Engineering, University of California, Berkeley (1984).

9. J. M. Kelly and J. L. Sackman, "Response spectra design methods for tuned equipment-structure systems", *Journal of Sound and Vibration*, **59**, (2), 171-179 (1978).

10. J. L. Sackman and J. M. Kelly, "Seismic analysis of internal equipment and components in structures", *Engineering Structures*, **1**, 179-190 (1979).

11. E. L. Wilson, A. Der Kiureghian and E. P. Bayo, "A replacement for the SRSS method in seismic analysis", *Earthquake Engineering and Structural Dynamics*, **9**, 187-194 (1981).

12. A. Der Kiureghian, "A response spectrum method for random vibration analysis of MDF systems", *Earthquake Engineering and Structural Dynamics*, **9**, 419-435 (1981).

13. C. J. Derham, J. M. Eidinger, J. M. Kelly and A. G. Thomas, "Natural rubber foundation bearings for earthquake protection - experimental results", *Natural Rubber Technology*, **8**, (3), 41-61 (1977).

(a) Fixed Base System

	El Cen	Taft	Parkfd	Pac Dm	Mean	Std Dev
BASE	4.407	0.866	1.688	2.497	2.365	1.313
FL. 5	4.371	3.060	2.599	4.367	3.599	0.787
OSC. 1	9.300	9.384	6.585	6.793	8.016	1.329
OSC. 2	7.063	8.771	4.826	6.833	6.873	1.399
OSC. 3	5.263	6.955	6.642	9.764	7.156	1.635

(b) No-lead Bearing System

	El Cen	Taft	Parkfd	Pac Dm	Mean	Std Dev
BASE	0.132	0.231	0.261	0.093	0.179	0.069
FL. 5	0.152	0.262	0.299	0.122	0.209	0.074
OSC. 1	0.349	0.472	0.581	0.480	0.471	0.082
OSC. 2	0.483	0.852	0.669	0.577	0.645	0.136
OSC. 3	0.469	0.683	0.720	0.534	0.602	0.103

(c) Lead Bearing System

	El Cen	Taft	Parkfd	Pac Dm	Mean	Std Dev
BASE	0.324	0.485	0.849	0.354	0.503	0.209
FL. 5	0.442	0.611	0.958	0.519	0.633	0.197
OSC. 1	1.890	1.764	3.344	1.469	2.120	0.725
OSC. 2	4.454	5.618	5.072	1.888	4.258	1.429
OSC. 3	3.173	2.725	2.642	2.170	2.678	0.356

Table 2 Statistical Values of Magnification Ratios
for Horizontal Only Excitations

(a) El Centro Record, Span: H=300, V=0 (Unit: g)

	TABLE	BASE	FL. 5	OSC. 1	OSC. 2	OSC. 3
Fixed Base	0.820	3.614	3.584	7.626	5.792	4.316
No-lead Bearing	0.835	0.110	0.127	0.291	0.403	0.392
Lead Bearing	0.851	0.276	0.376	1.608	3.790	2.700

(b) Taft Record, Span: H=350, V=0 (Unit: g)

	TABLE	BASE	FL. 5	OSC. 1	OSC. 2	OSC. 3
Fixed Base	0.536	0.464	1.640	5.030	4.701	3.728
No-lead Bearing	0.562	0.130	0.147	0.265	0.479	0.384
Lead Bearing	0.581	0.282	0.355	1.025	3.264	1.583

(c) Parkfield Record, Span: H=300, V=0 (Unit: g)

	TABLE	BASE	FL. 5	OSC. 1	OSC. 2	OSC. 3
Fixed Base	0.581	0.981	1.510	3.826	2.804	3.859
No-lead Bearing	0.375	0.098	0.112	0.218	0.251	0.270
Lead Bearing	0.377	0.320	0.361	1.261	1.912	0.996

(d) Pacoima Dam Record, Span: H=300, V=0 (Unit: g)

	TABLE	BASE	FL. 5	OSC. 1	OSC. 2	OSC. 3
Fixed Base	1.042	2.602	4.550	7.078	7.120	10.174
No-lead Bearing	1.292	0.120	0.157	0.620	0.746	0.690
Lead Bearing	1.330	0.471	0.690	1.954	2.511	2.886

Table 1 Peak Accelerations of Frame and Oscillators for Horizontal Only Excitations

(a) El Centro Record, Span: H=200, V=200 (Unit: g)

	TABLE	BASE	FL. 5	OSC. 1	OSC. 2	OSC. 3
Fixed Base	0.559	4.270	1.703	4.337	3.756	3.073
No-lead Bearing	0.562	0.171	0.208	0.370	1.051	2.009
Lead Bearing	0.543	0.260	0.345	1.207	2.334	3.054

(b) Taft Record, Span: H=350, V=350 (Unit: g)

	TABLE	BASE	FL. 5	OSC. 1	OSC. 2	OSC. 3
Fixed Base	0.536	0.464	1.640	5.030	4.701	3.728
No-lead Bearing	0.527	0.173	0.225	0.324	0.856	1.239
Lead Bearing	0.548	0.322	0.336	1.016	3.089	2.054

(c) Pacoima Dam Record, Span: H=300, V=200 (Unit: g)

	TABLE	BASE	FL. 5	OSC. 1	OSC. 2	OSC. 3
Fixed Base	1.042	2.602	4.550	7.078	7.120	10.174
No-lead Bearing	1.287	0.210	0.220	0.537	1.301	2.012
Lead Bearing	1.282	0.466	0.716	1.728	2.613	3.761

Table 4 Peak Accelerations of Frame and Oscillators for Combined Horizontal and Vertical Excitations

(a) Oscillator 1

	El Cen	Taft	Parkfd	Pac Dm	Mean	Std Dev
No-lead Bearing	26.21	18.98	17.55	11.42	18.54	6.074
Lead Bearing	4.743	4.907	3.034	3.622	4.077	0.900

(b) Oscillator 2

	El Cen	Taft	Parkfd	Pac Dm	Mean	Std Dev
No-lead Bearing	14.37	9.814	11.17	9.544	11.22	1.918
Lead Bearing	1.528	1.440	1.467	2.836	1.818	0.680

(c) Oscillator 3

	El Cen	Taft	Parkfd	Pac Dm	Mean	Std Dev
No-lead Bearing	11.07	9.708	14.29	14.74	12.44	2.464
Lead Bearing	1.699	2.355	3.874	3.525	2.838	1.051

Table 3 Statistical Values of Reduction Factors for Horizontal Only Excitations

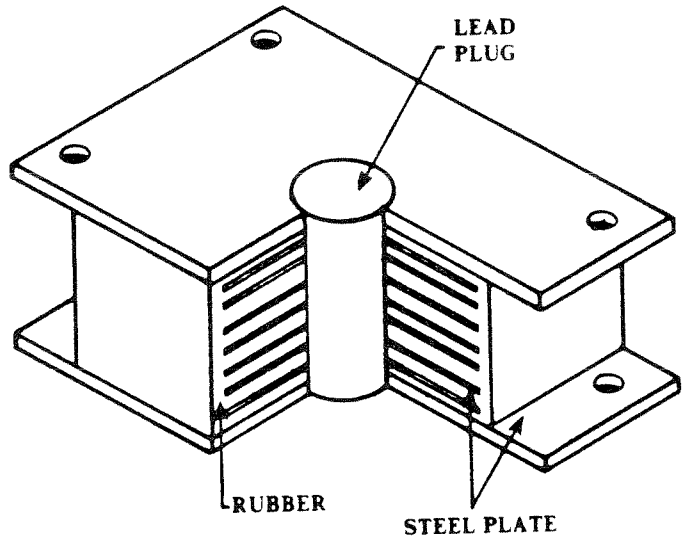

Figure 1 Lead-Rubber Hysteretic Bearing

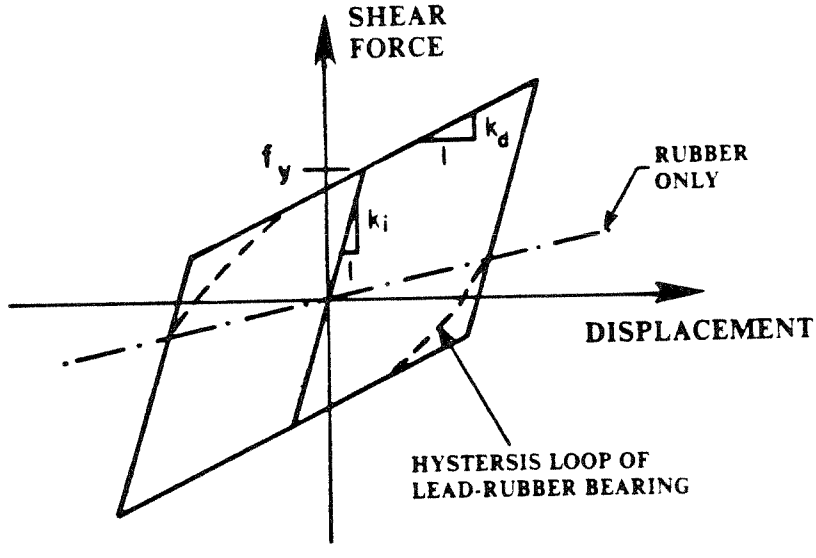

Figure 2 Bilinear Force-Displacement Relation

(a) El Centro Record, Span: H=200, V=200

	Magnification Ratio			Reduction Factor		
	OSC. 1	OSC. 2	OSC. 3	OSC. 1	OSC. 2	OSC. 3
No-lead Bearing	0.658	1.870	3.574	11.72	3.574	1.530
Lead Bearing	2.223	4.298	5.624	3.593	1.609	1.006

(b) Taft Record, Span: H=350, V=350

	Magnification Ratio			Reduction Factor		
	OSC. 1	OSC. 2	OSC. 3	OSC. 1	OSC. 2	OSC. 3
No-lead Bearing	0.615	1.624	2.351	15.52	5.492	3.009
Lead Bearing	1.854	5.637	3.748	4.951	1.522	1.815

(c) Pacoima Dam Record, Span: H=300, V=200

	Magnification Ratio			Reduction Factor		
	OSC. 1	OSC. 2	OSC. 3	OSC. 1	OSC. 2	OSC. 3
No-lead Bearing	0.417	1.011	1.563	13.18	5.473	5.057
Lead Bearing	1.348	2.038	2.934	4.096	2.725	2.705

Table 5 Magnification Ratios and Reduction Factors for Combined Horizontal and Vertical Excitations

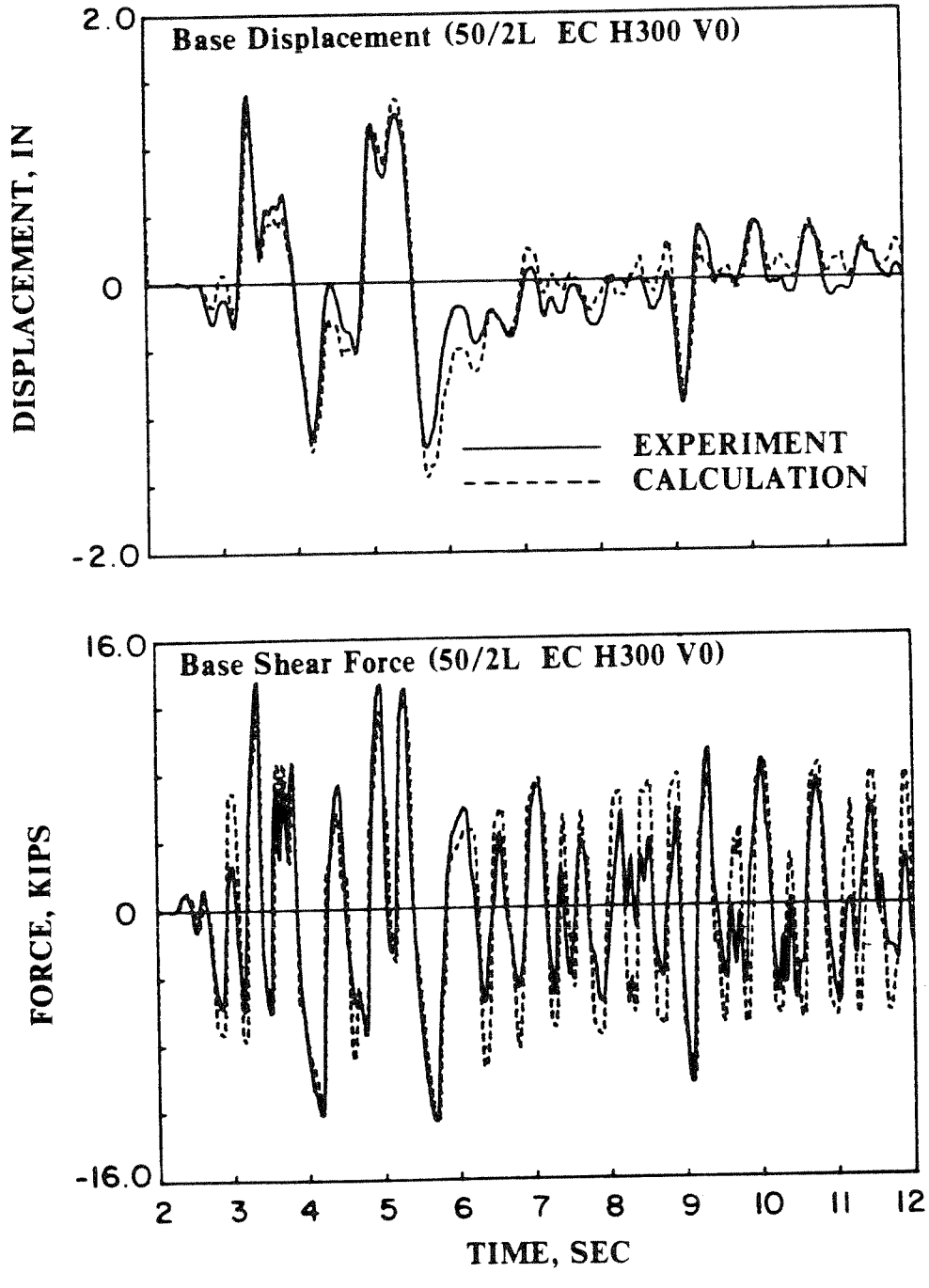

Figure 5 Base Displacement and Base Shear Force under El Centro Earthquake

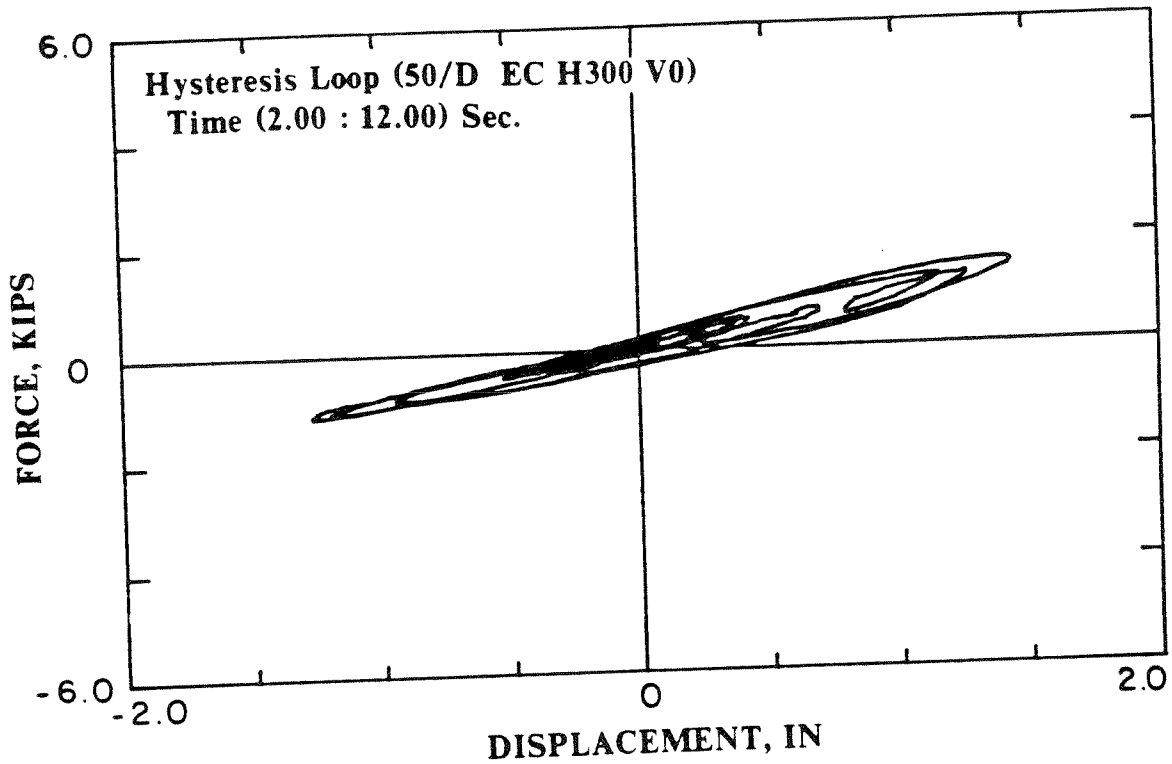

Figure 3 Hysteresis Loop of Rubber Bearing without Lead

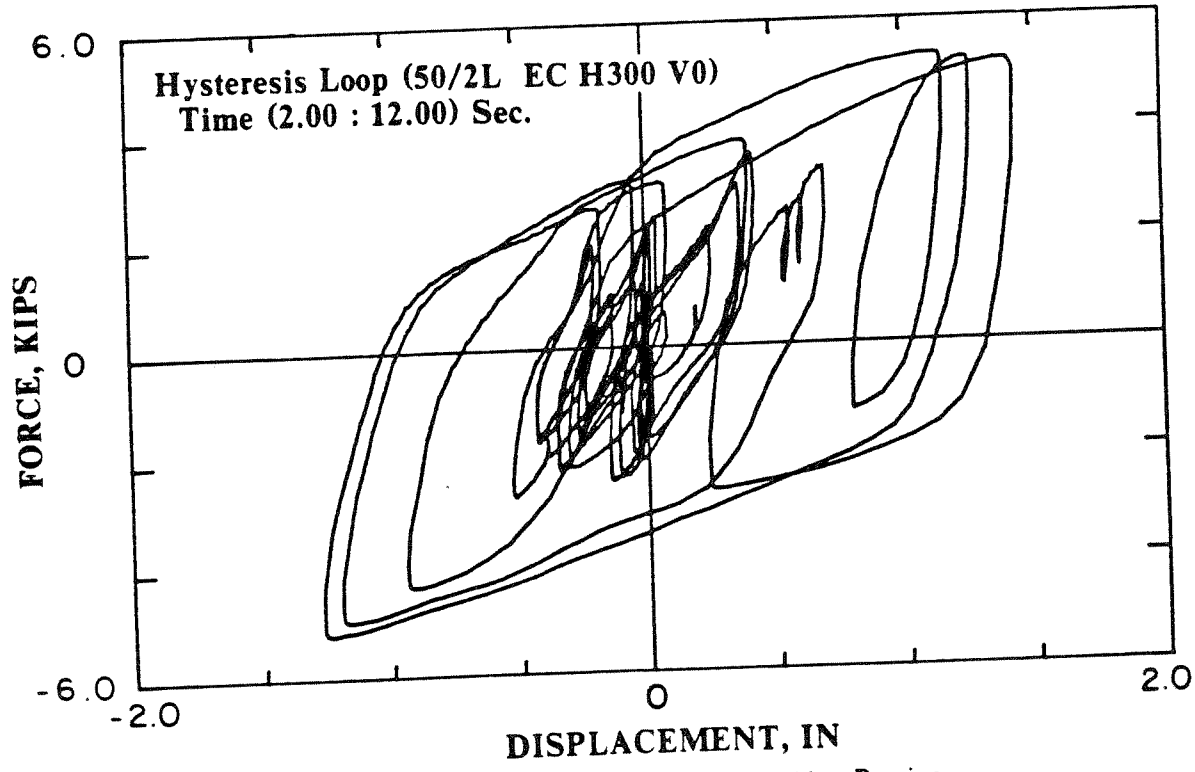

Figure 4 Hysteresis Loop of Lead-Rubber Bearing

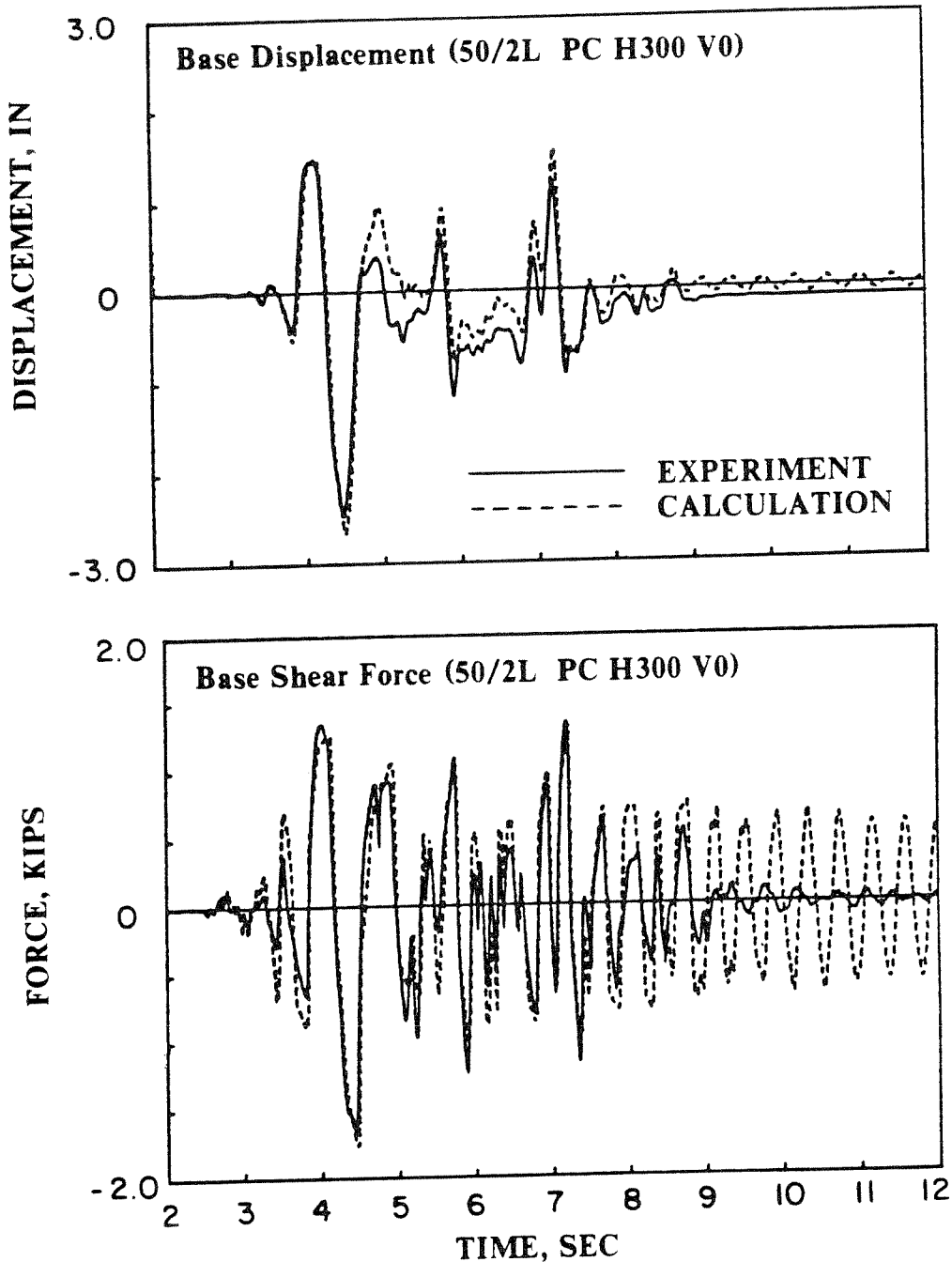

Figure 7 Base Displacement and Base Shear Force under Pacoima Dam Earthquake

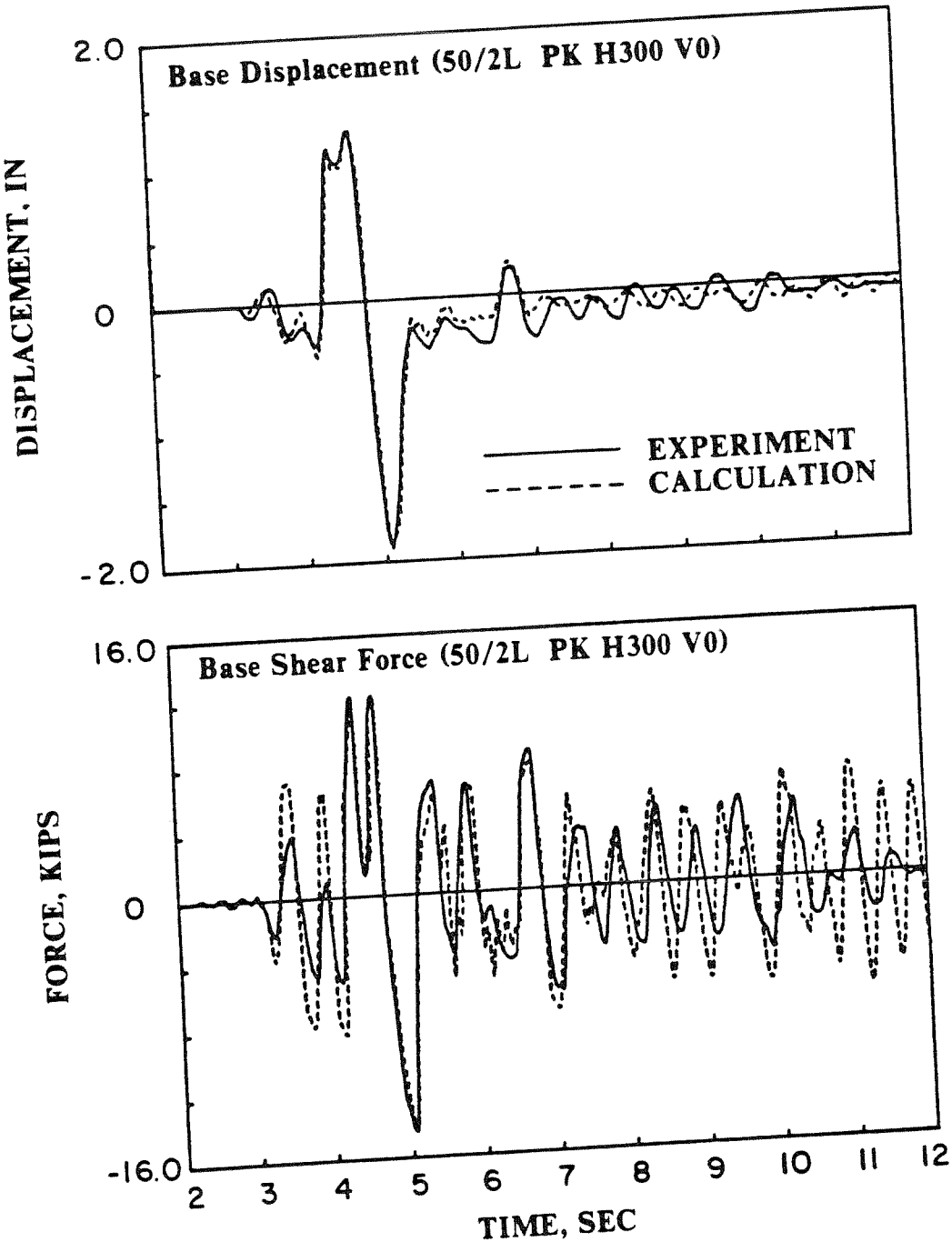

Figure 6 Base Displacement and Base Shear Force under Parkfield Earthquake

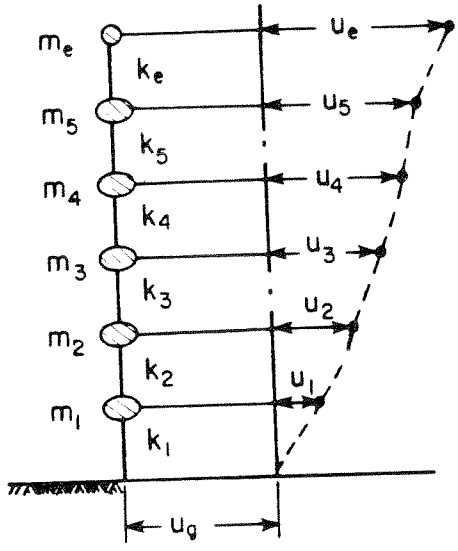

Figure 10 Theoretical Model of Equipment on Fixed Base Structure

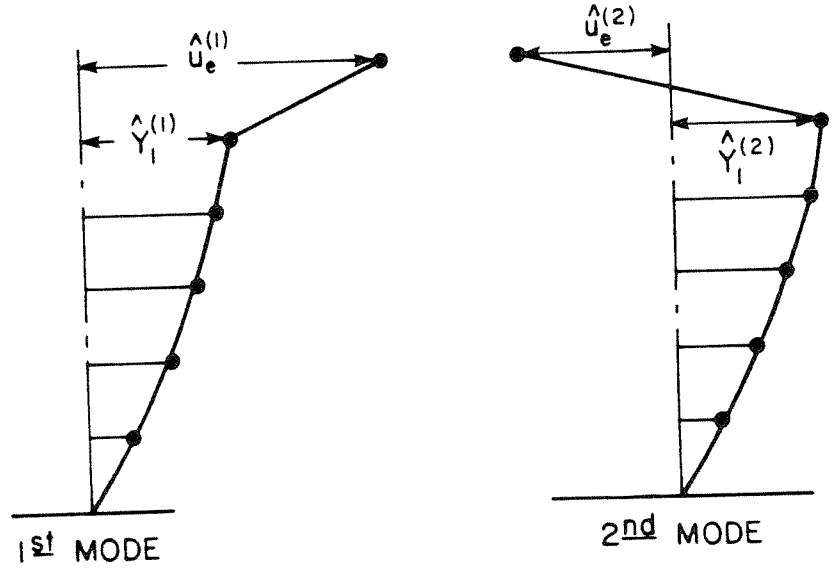

Figure 11 Mode Shapes of Fixed Base Structure with Tuned Equipment

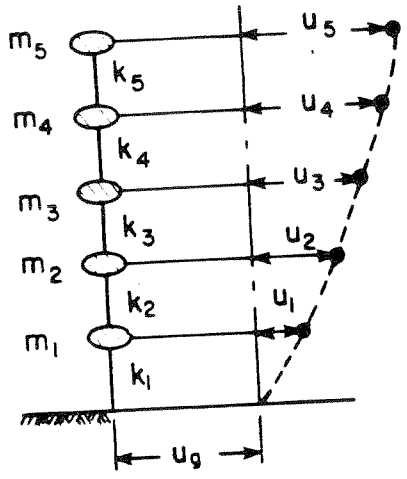

Figure 8 Theoretical Model of Fixed Base Structure

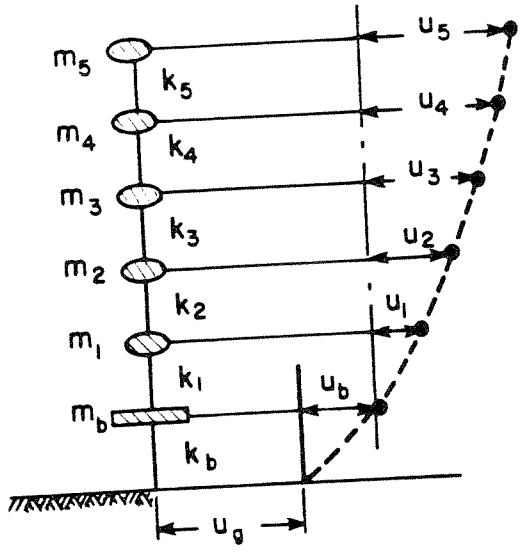

Figure 9 Theoretical Model of Base-Isolated Structure

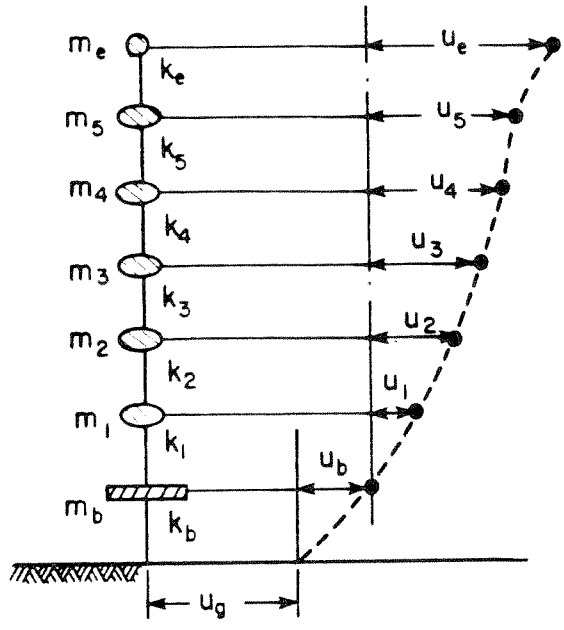

Figure 14 Theoretical Model of Equipment on Base-Isolated Structure

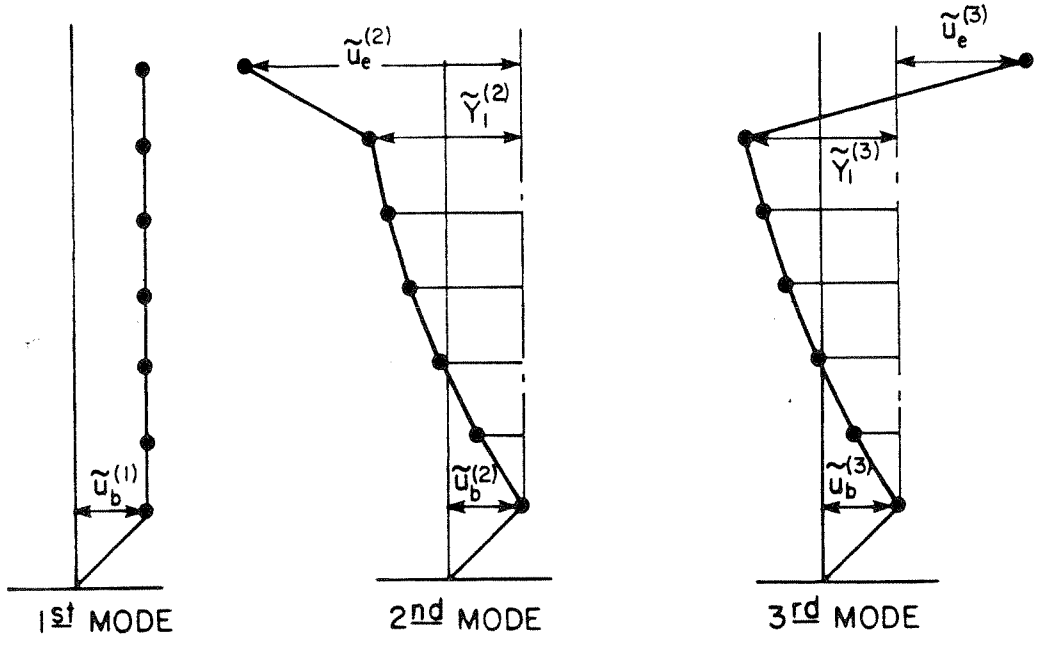

Figure 15 Mode Shapes of Base-Isolated Structure with Tuned Equipment

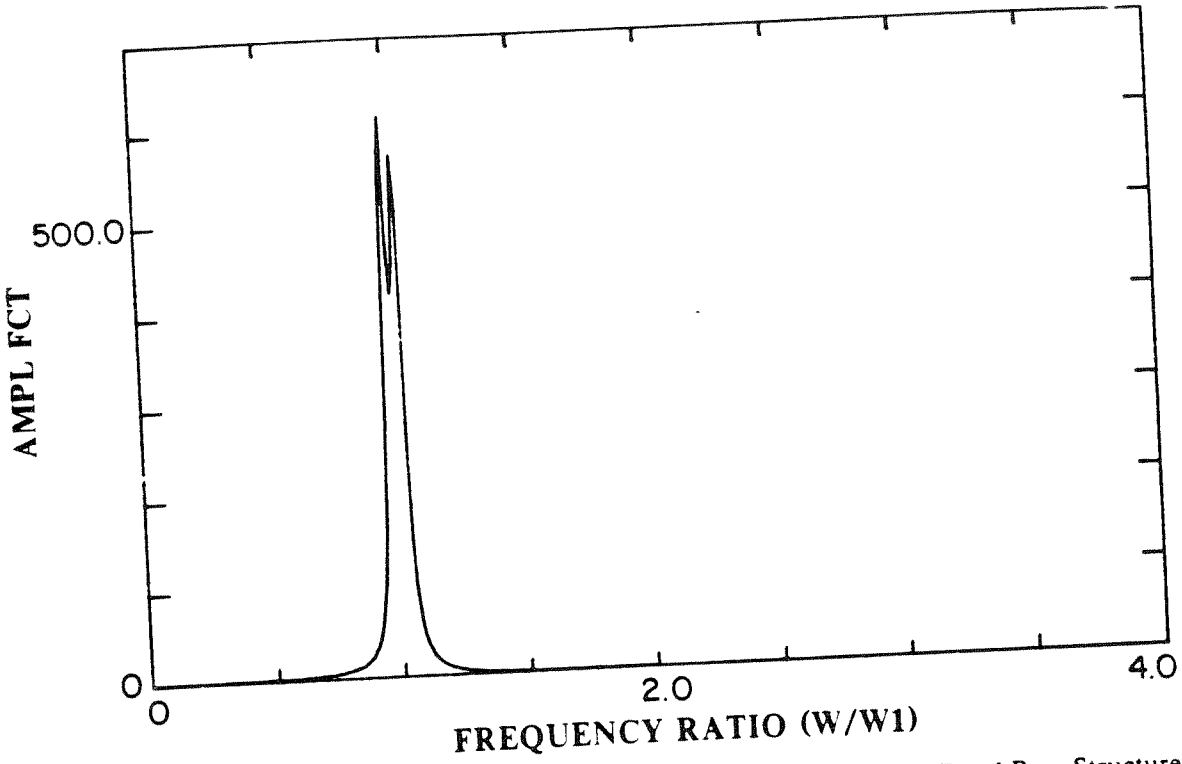

Figure 12 Amplification Factor Curve of Tuned Equipment on Fixed Base Structure

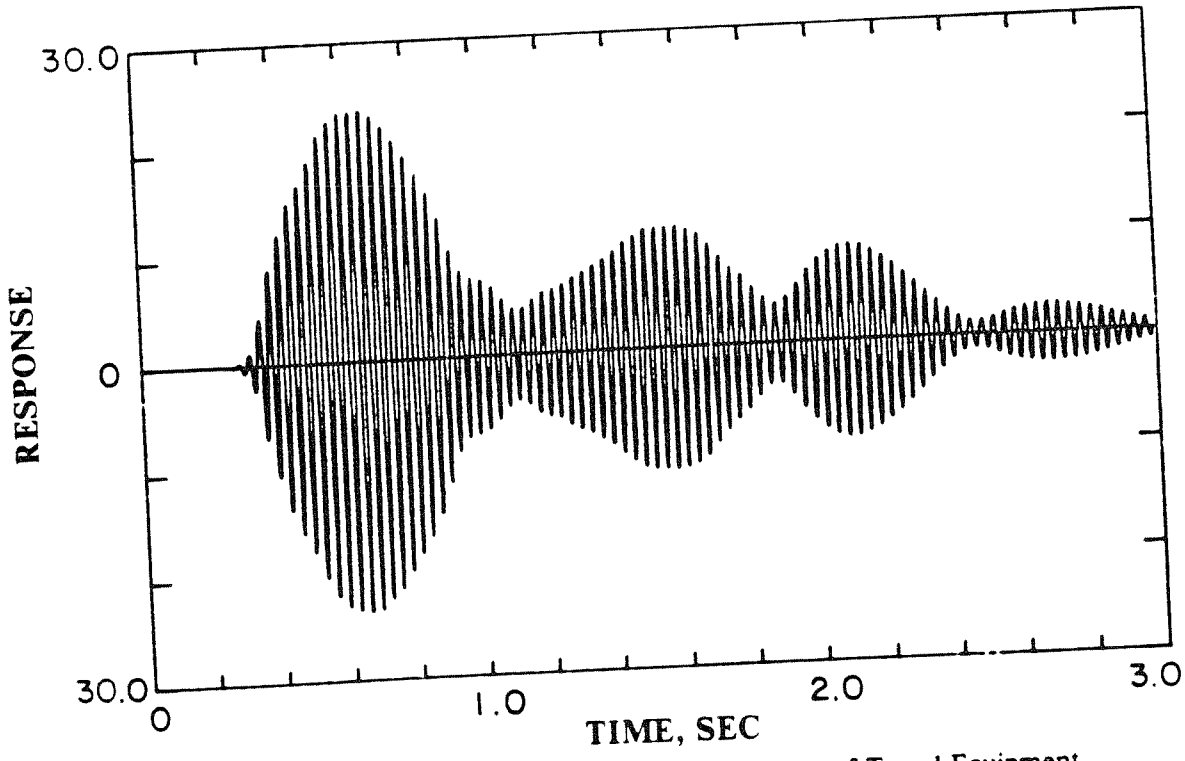

Figure 13 Calculated Acceleration Time History of Tuned Equipment on Fixed Base Structure

Figure 18 Experimental Model of Five-Story Steel Frame and Oscillators

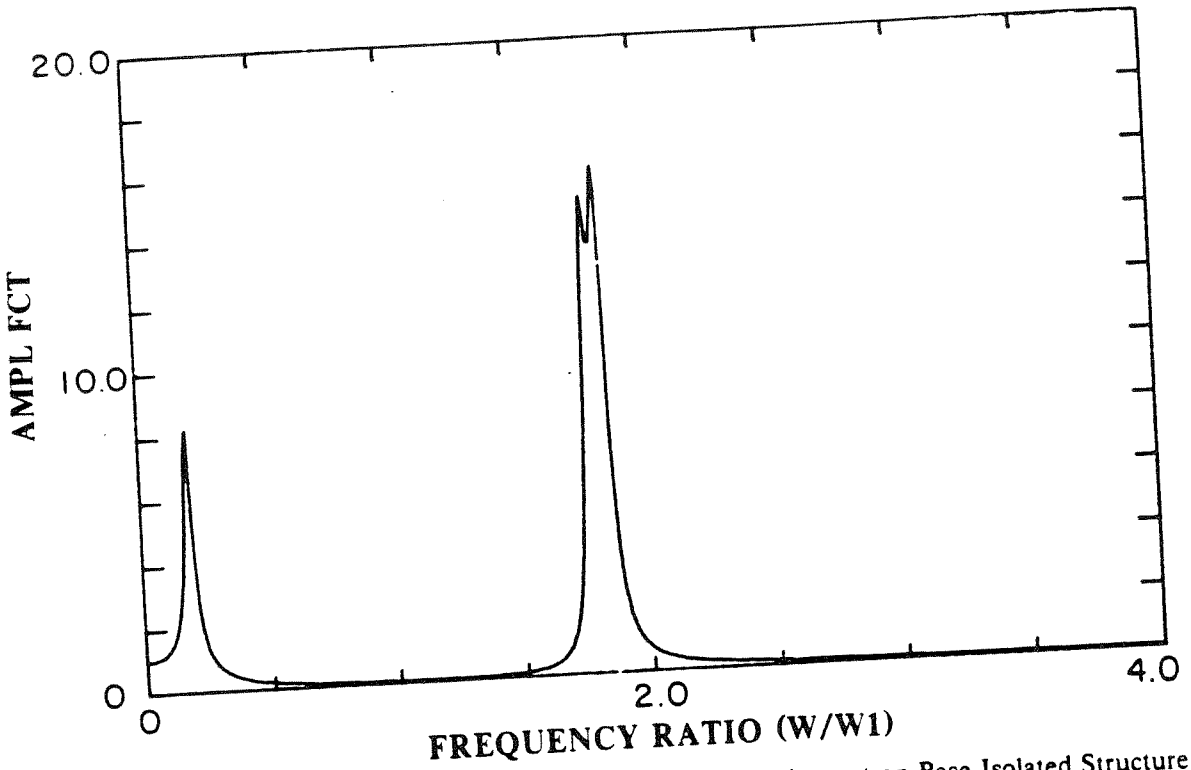

Figure 16 Amplification Factor Curve of Tuned Equipment on Base-Isolated Structure

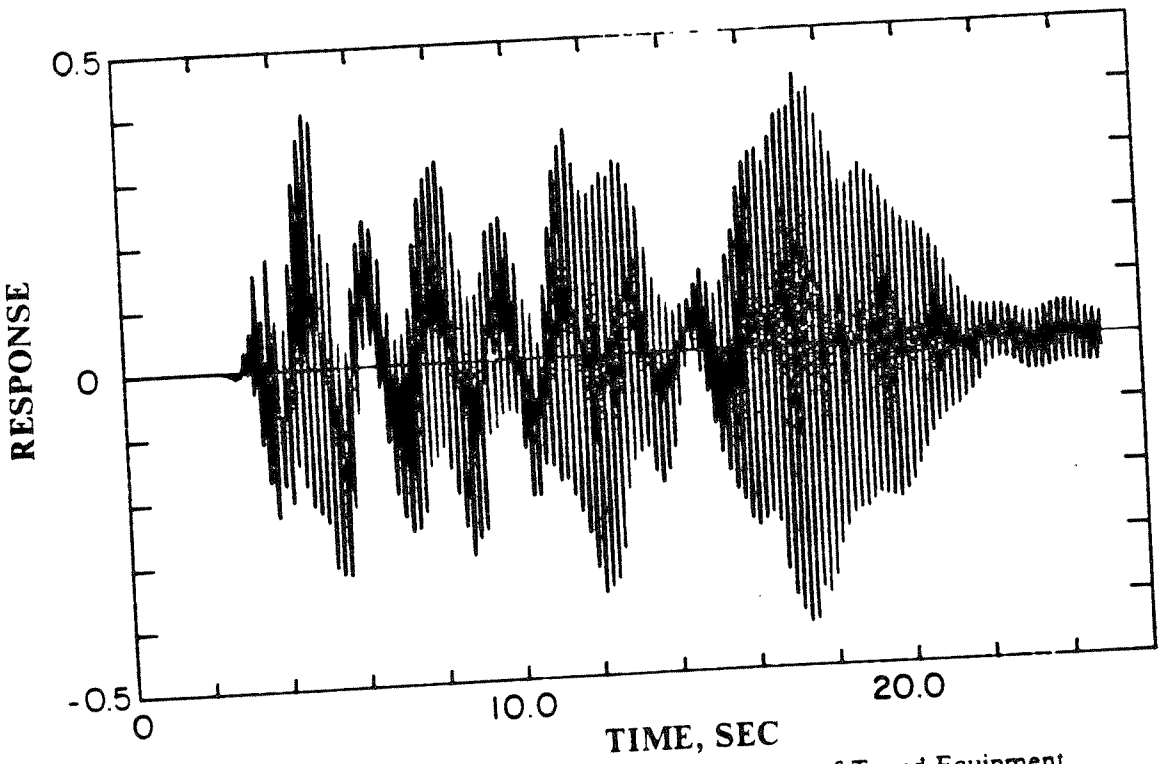

Figure 17 Calculated Acceleration Time History of Tuned Equipment on Base-Isolated Structure

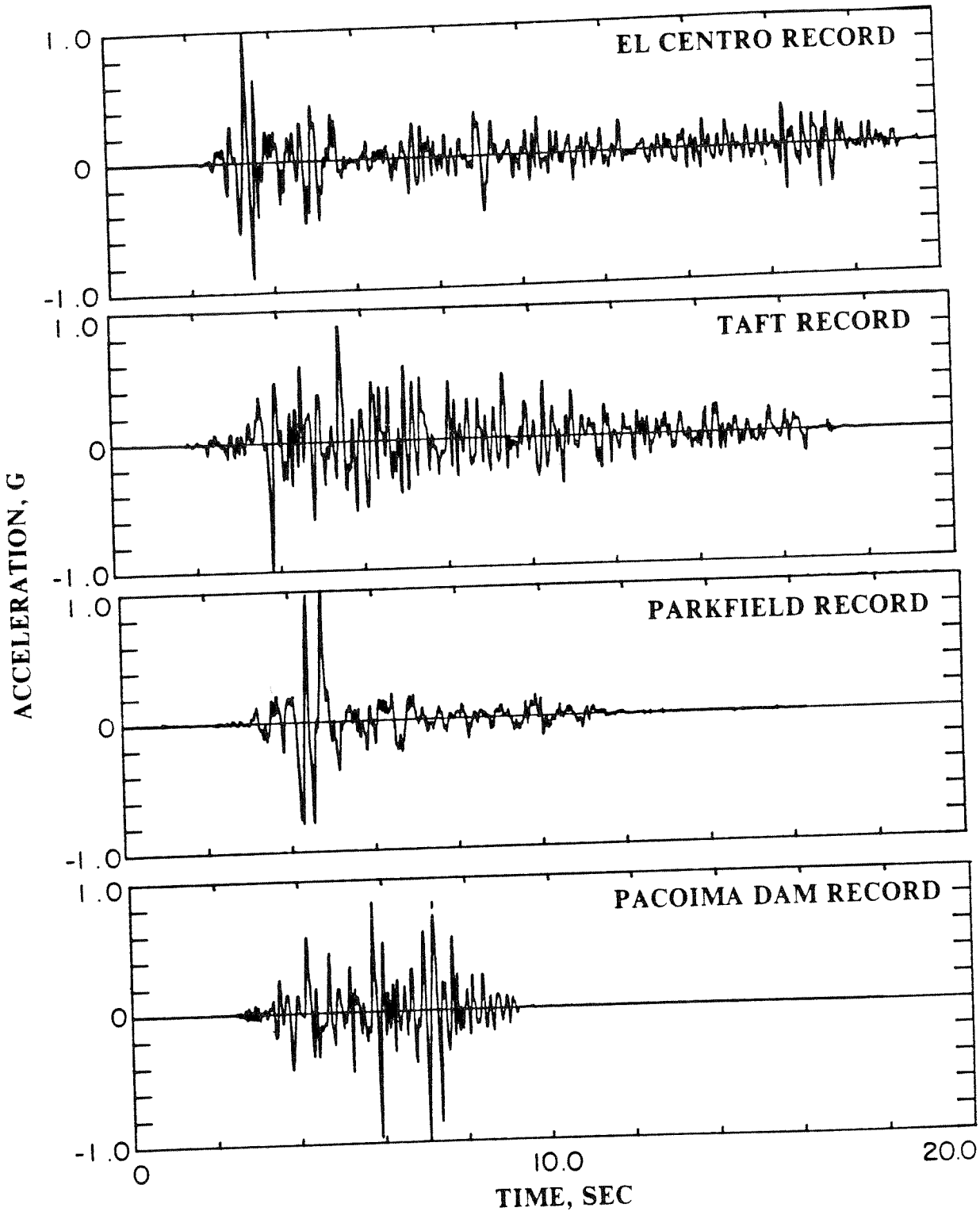

Figure 20 Time Histories of Normalized Time-Scaled Input Accelerations

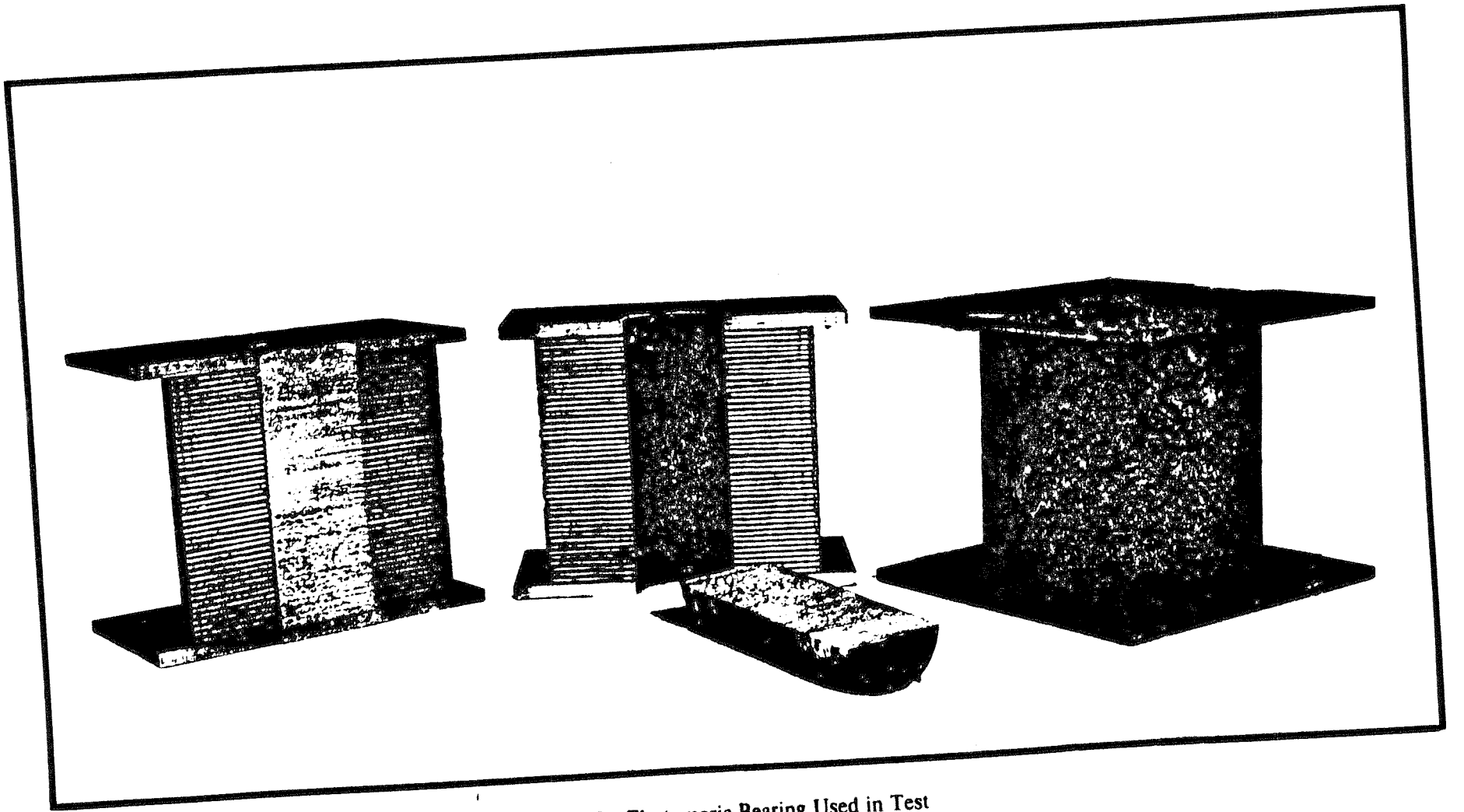

Figure 19 Elastomeric Bearing Used in Test

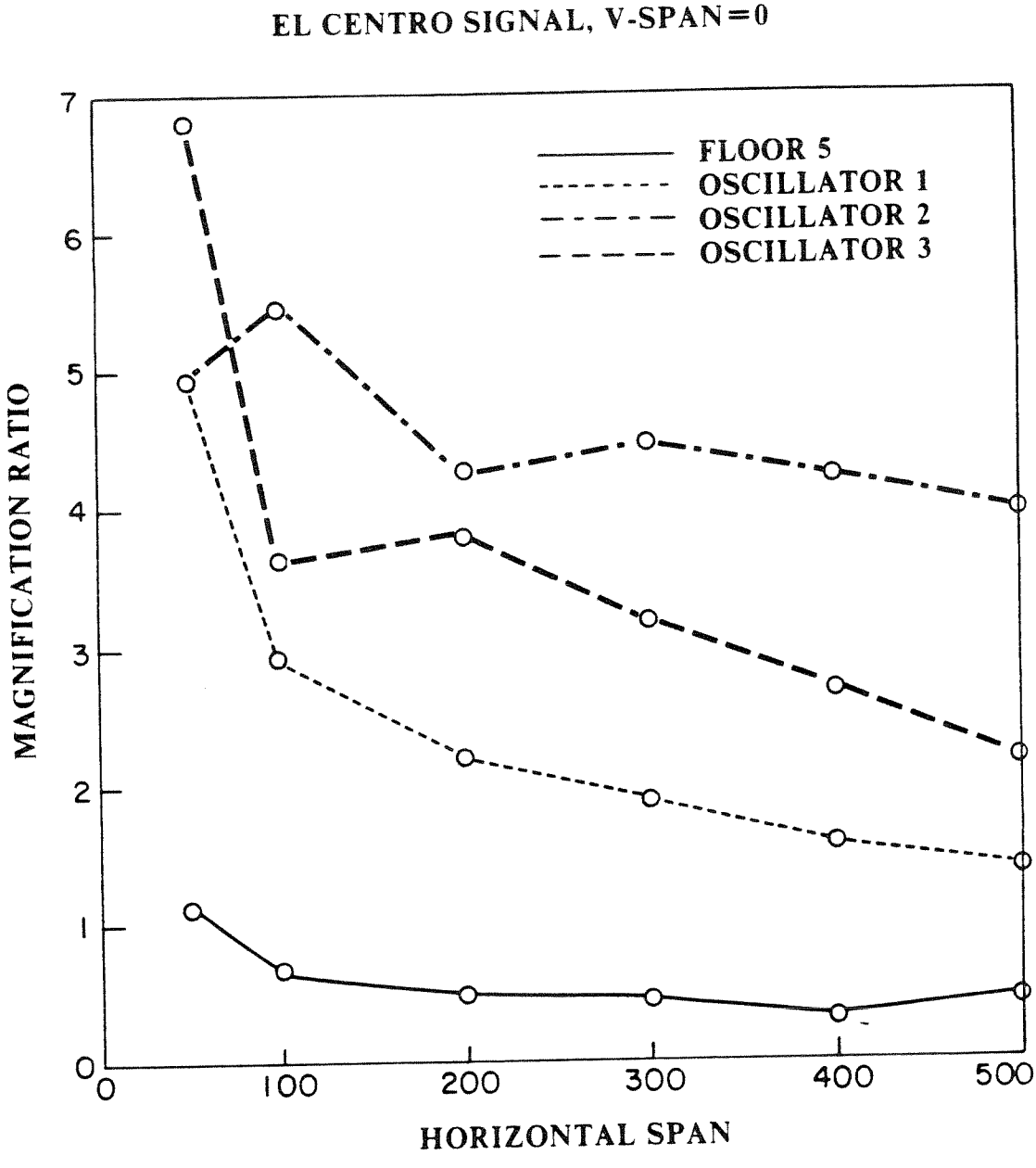

Figure 22 Magnification Ratios of Lead Bearing under Increasing Earthquake Intensity

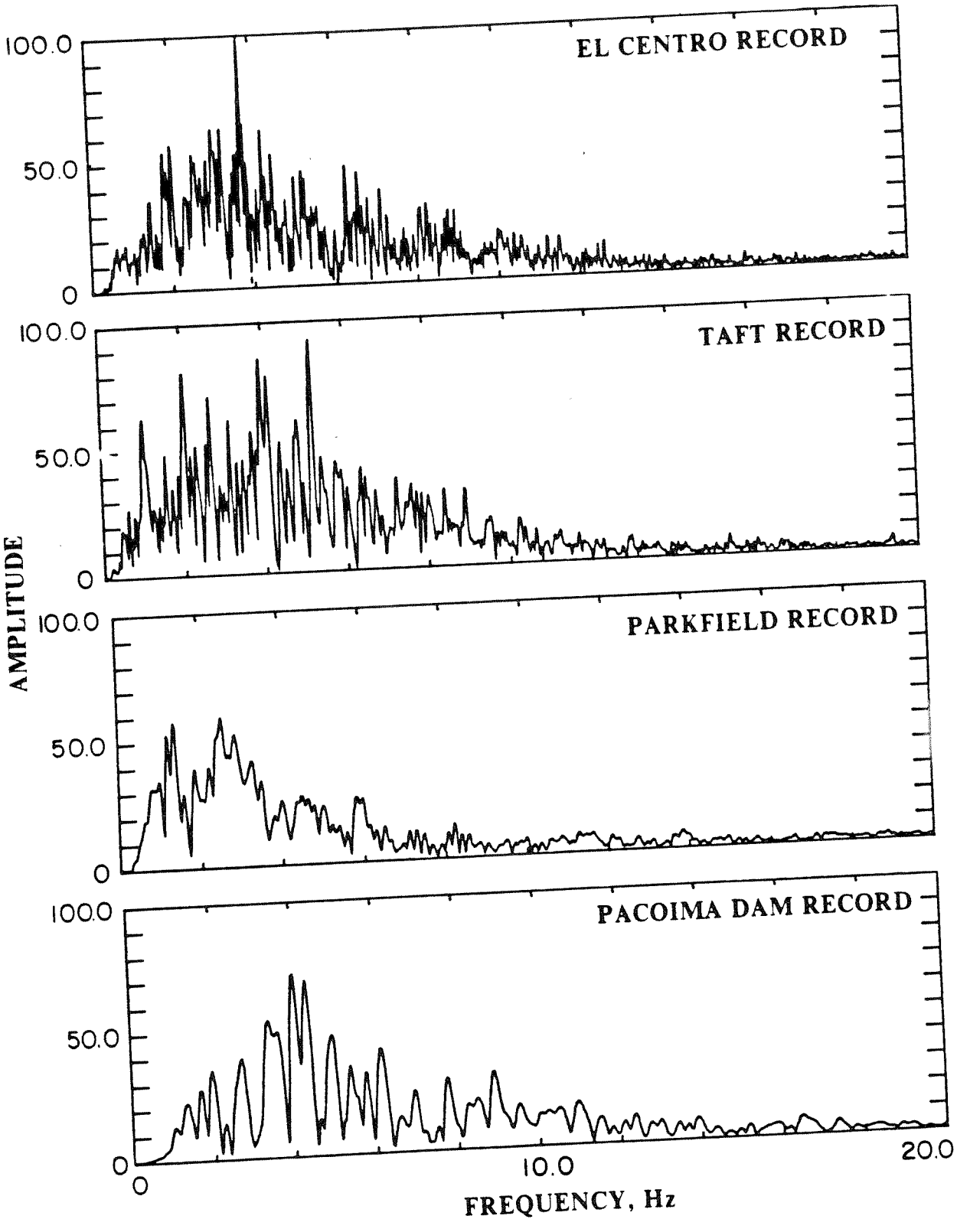

Figure 21 Fourier Spectra of Normalized Time-Scaled Input Accelerations

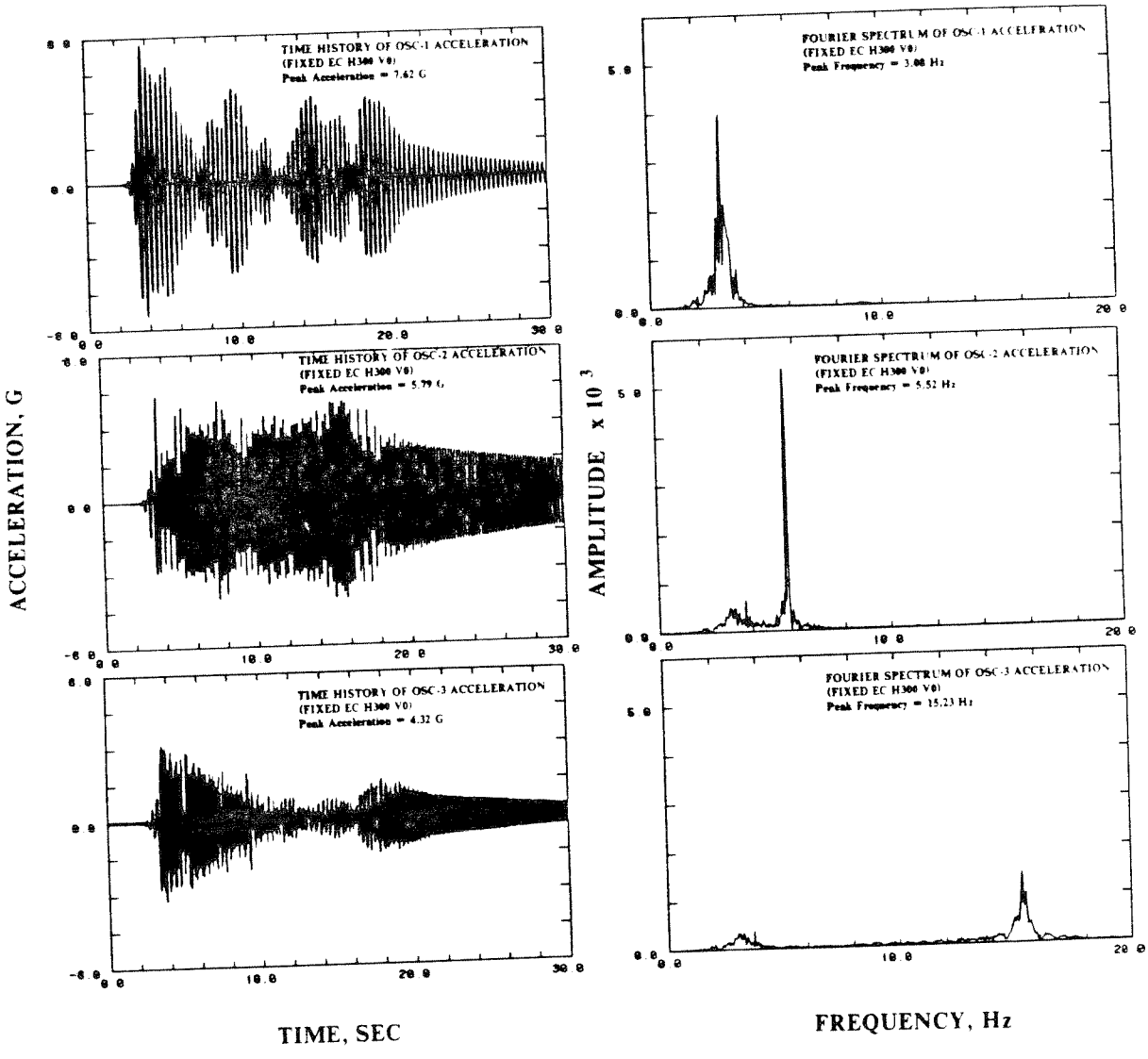

Figure 24 Acceleration Time Histories and Fourier Spectra of Oscillators on Fixed Base System under El Centro Earthquake

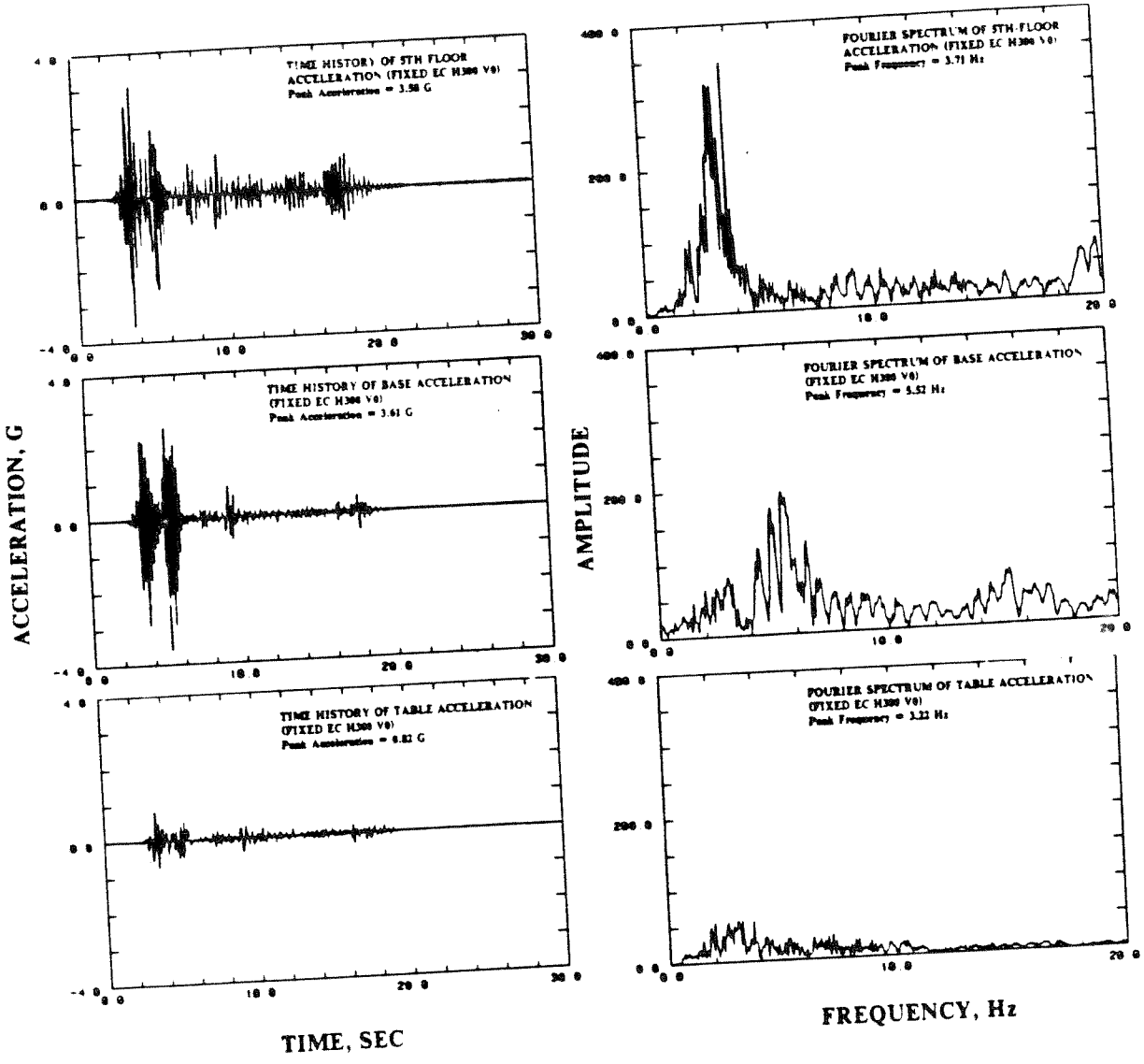

Figure 23 Acceleration Time Histories and Fourier Spectra of Frame in Fixed Base System under El Centro Earthquake

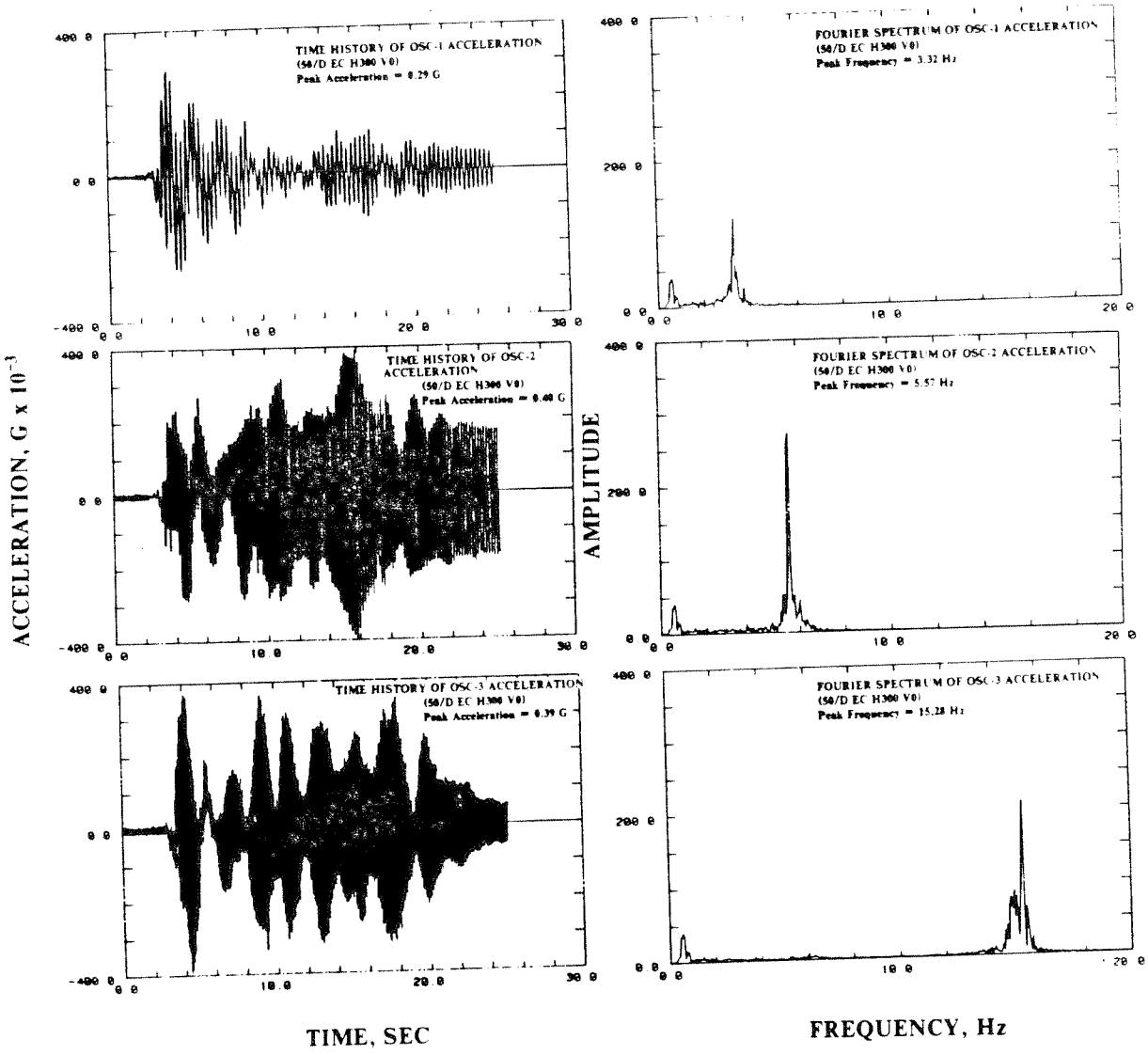

Figure 26 Acceleration Time Histories and Fourier Spectra of Oscillators on No-lead Bearing System under El Centro Earthquake

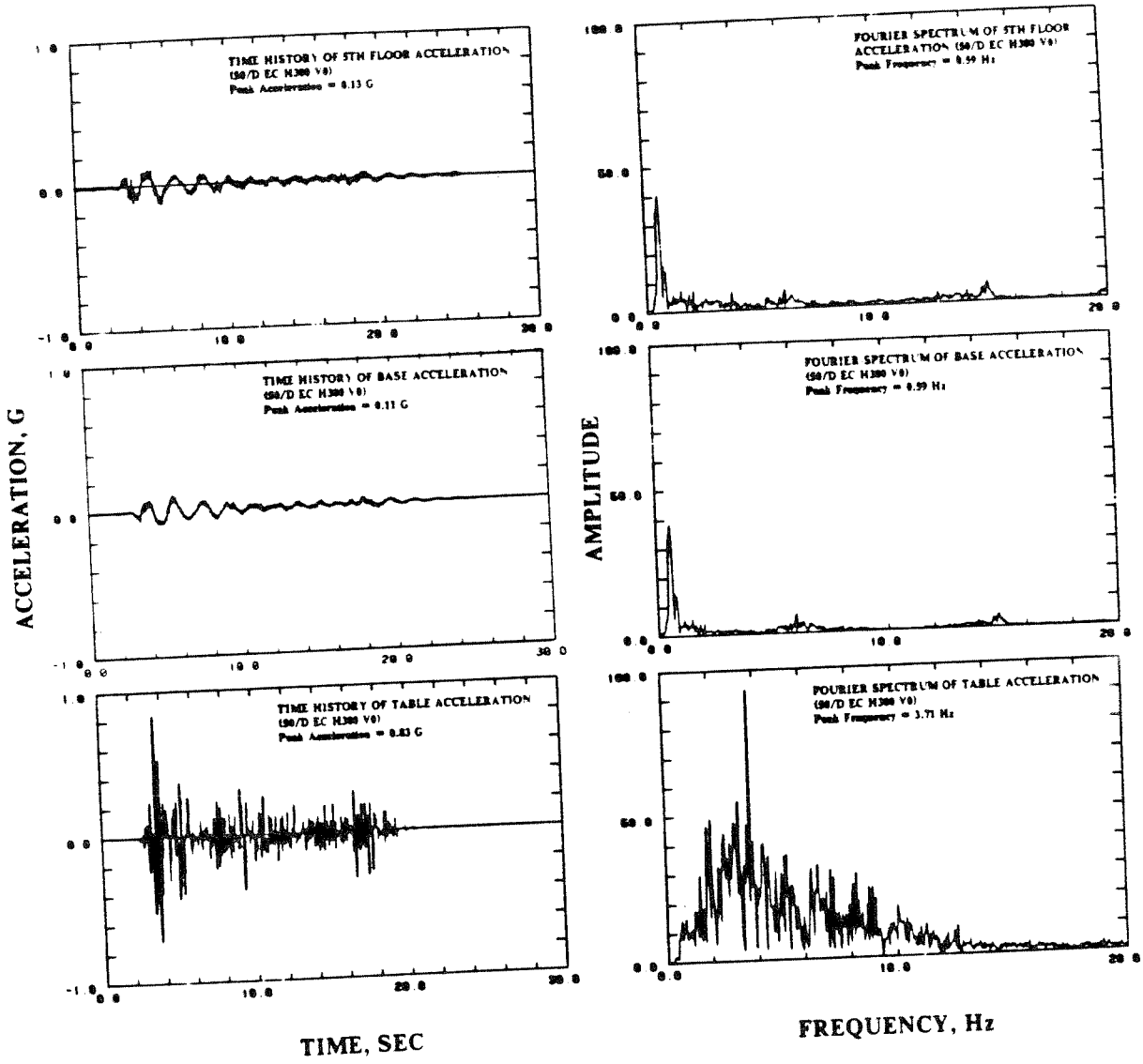

Figure 25 Acceleration Time Histories and Fourier Spectra of Frame in No-lead Bearing System under El Centro Earthquake

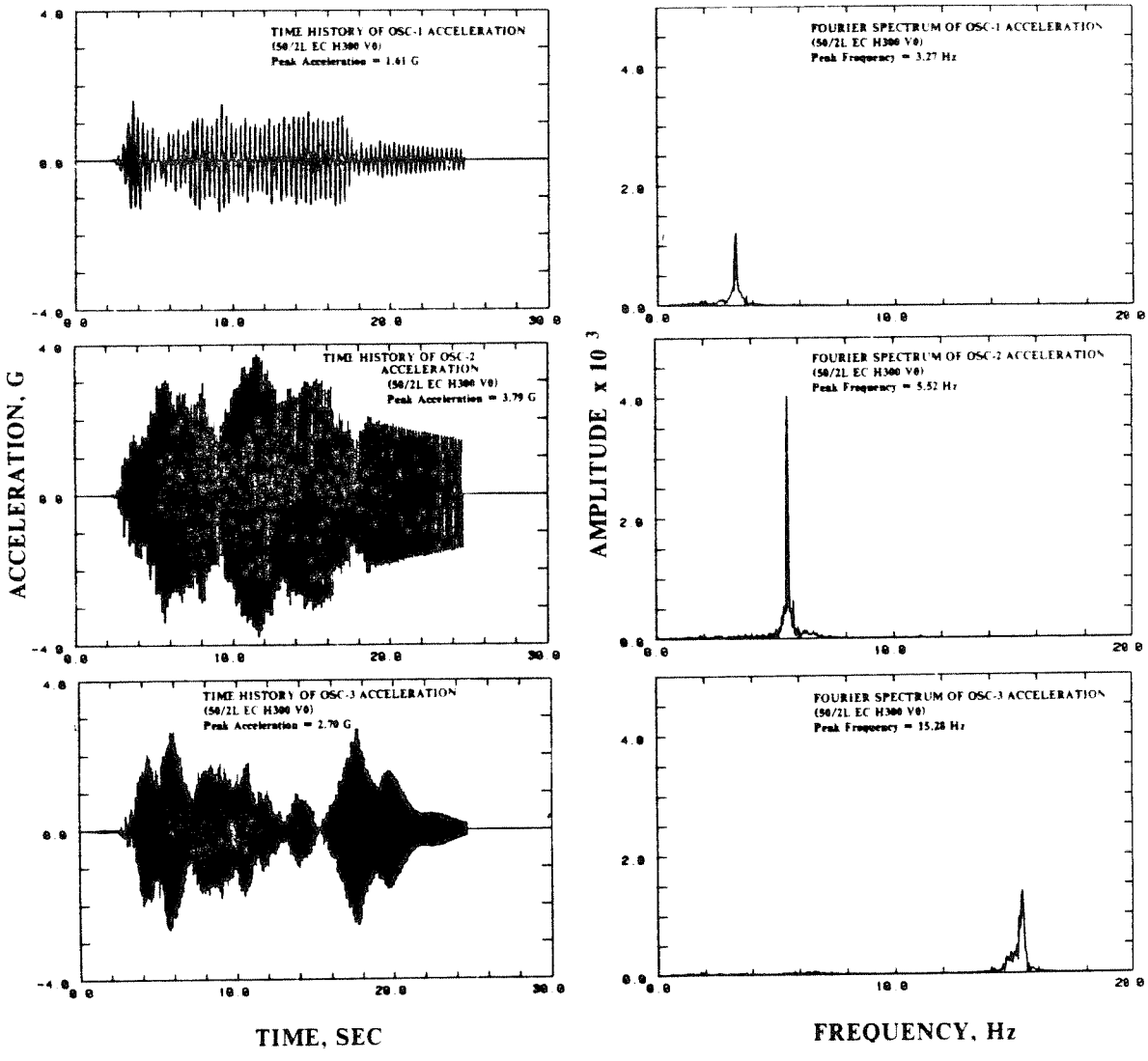

Figure 28 Acceleration Time Histories and Fourier Spectra of Oscillators on Lead Bearing System under El Centro Earthquake

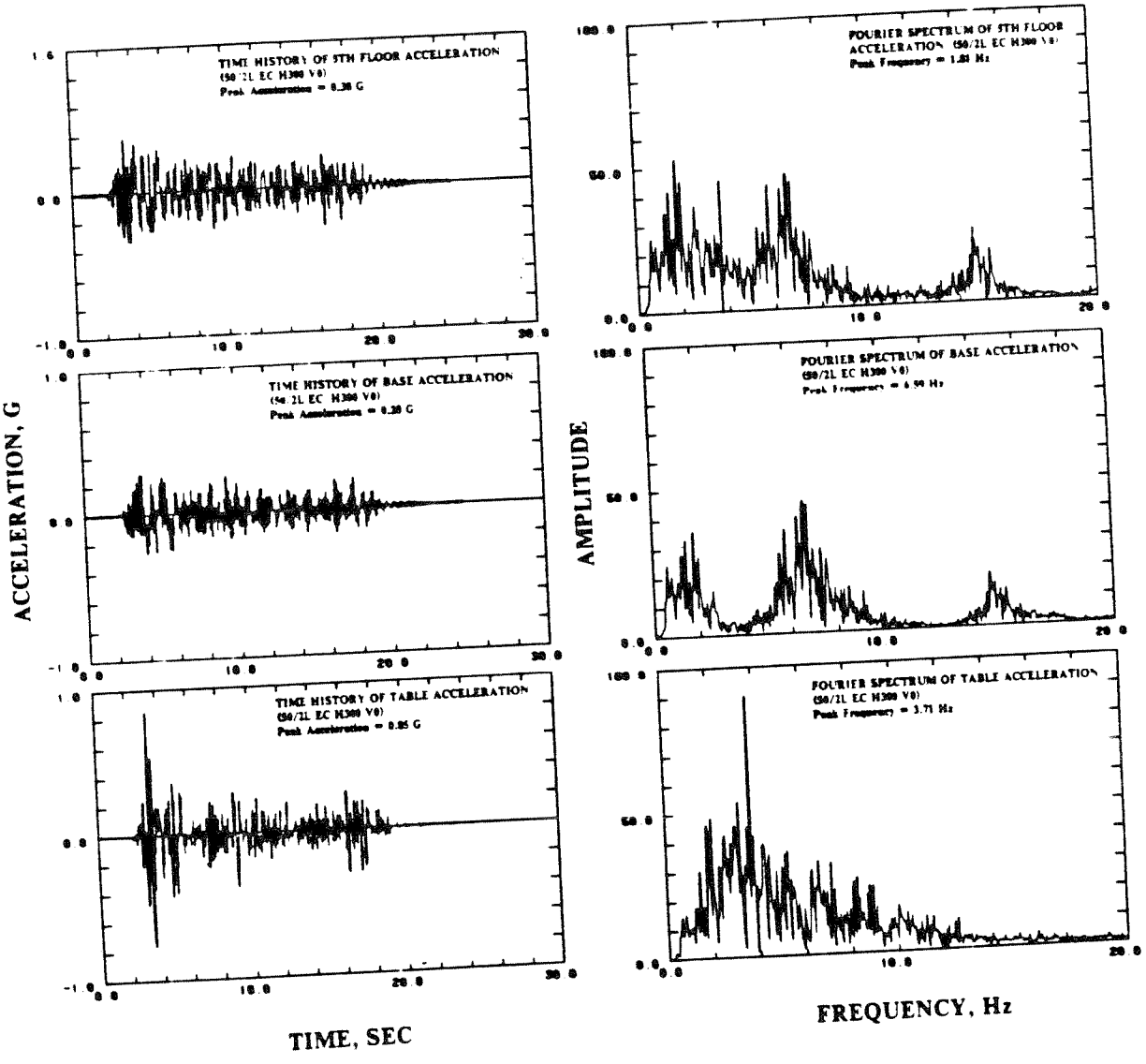

Figure 27 Acceleration Time Histories and Fourier Spectra of Frame in Lead Bearing System under El Centro Earthquake

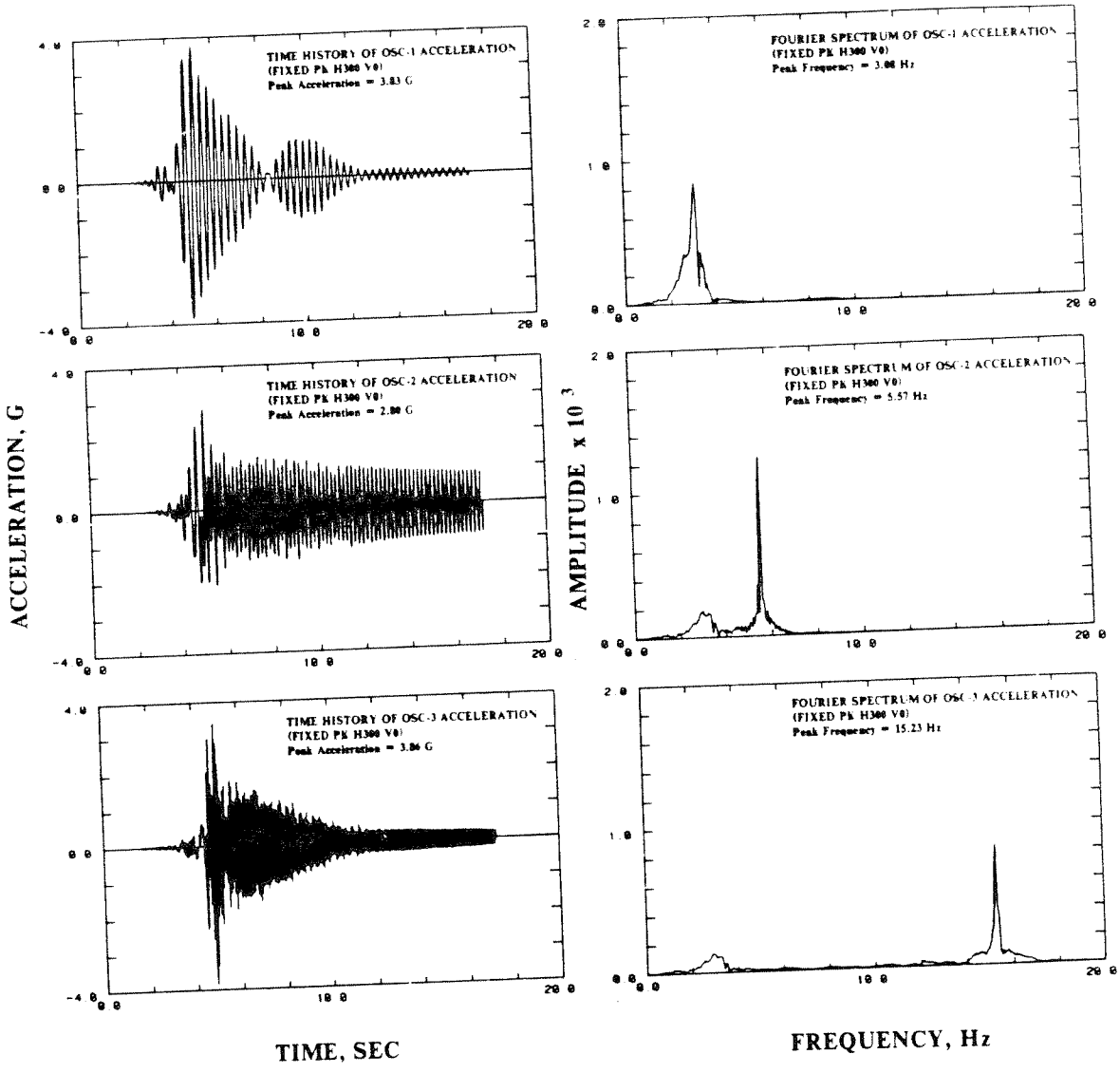

Figure 30 Acceleration Time Histories and Fourier Spectra of Oscillators on Fixed Base System under Parkfield Earthquake

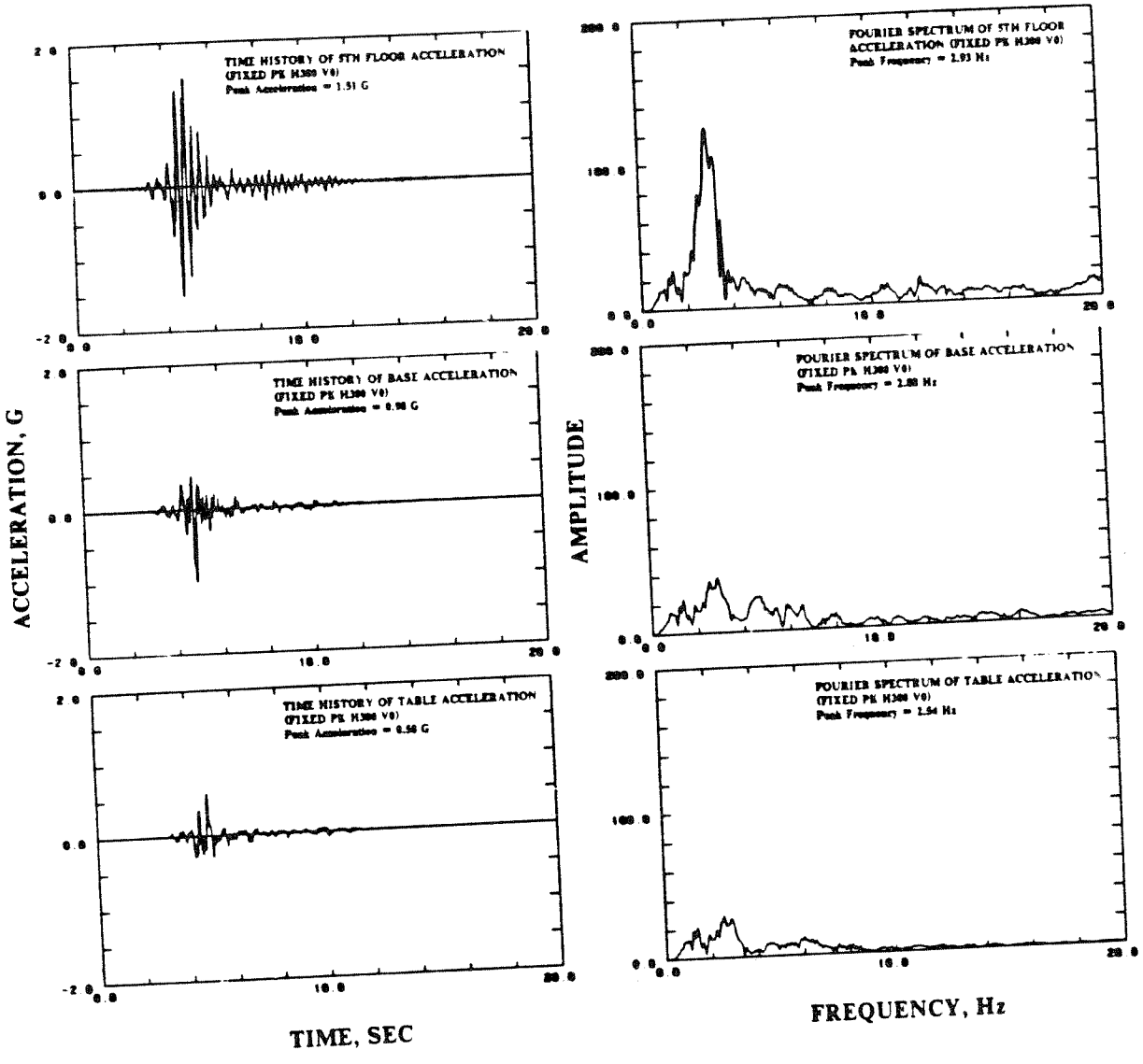

Figure 29 Acceleration Time Histories and Fourier Spectra of Frame in Fixed Base System under Parkfield Earthquake

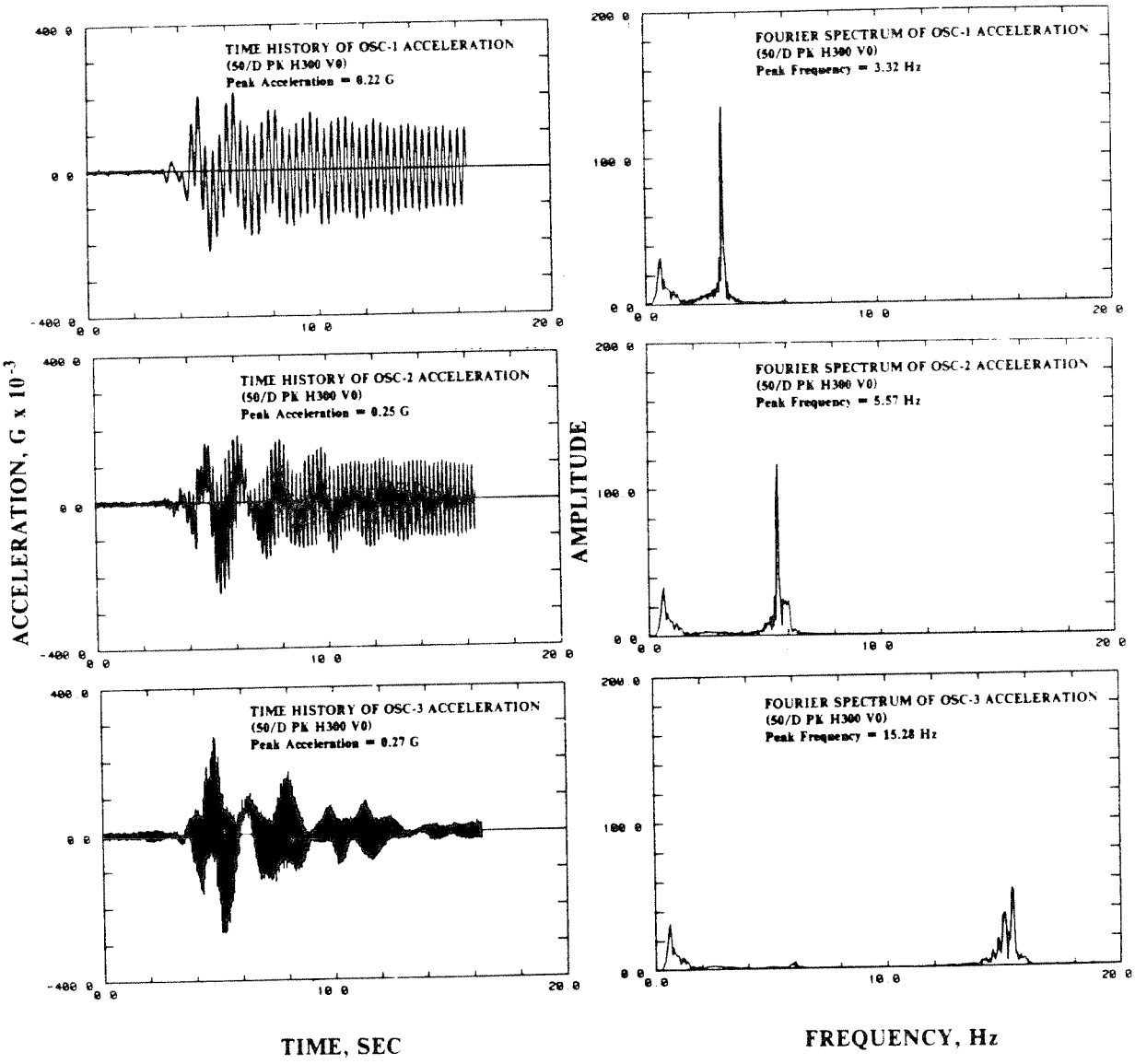

Figure 32 Acceleration Time Histories and Fourier Spectra of Oscillators on No-lead Bearing System under Parkfield Earthquake

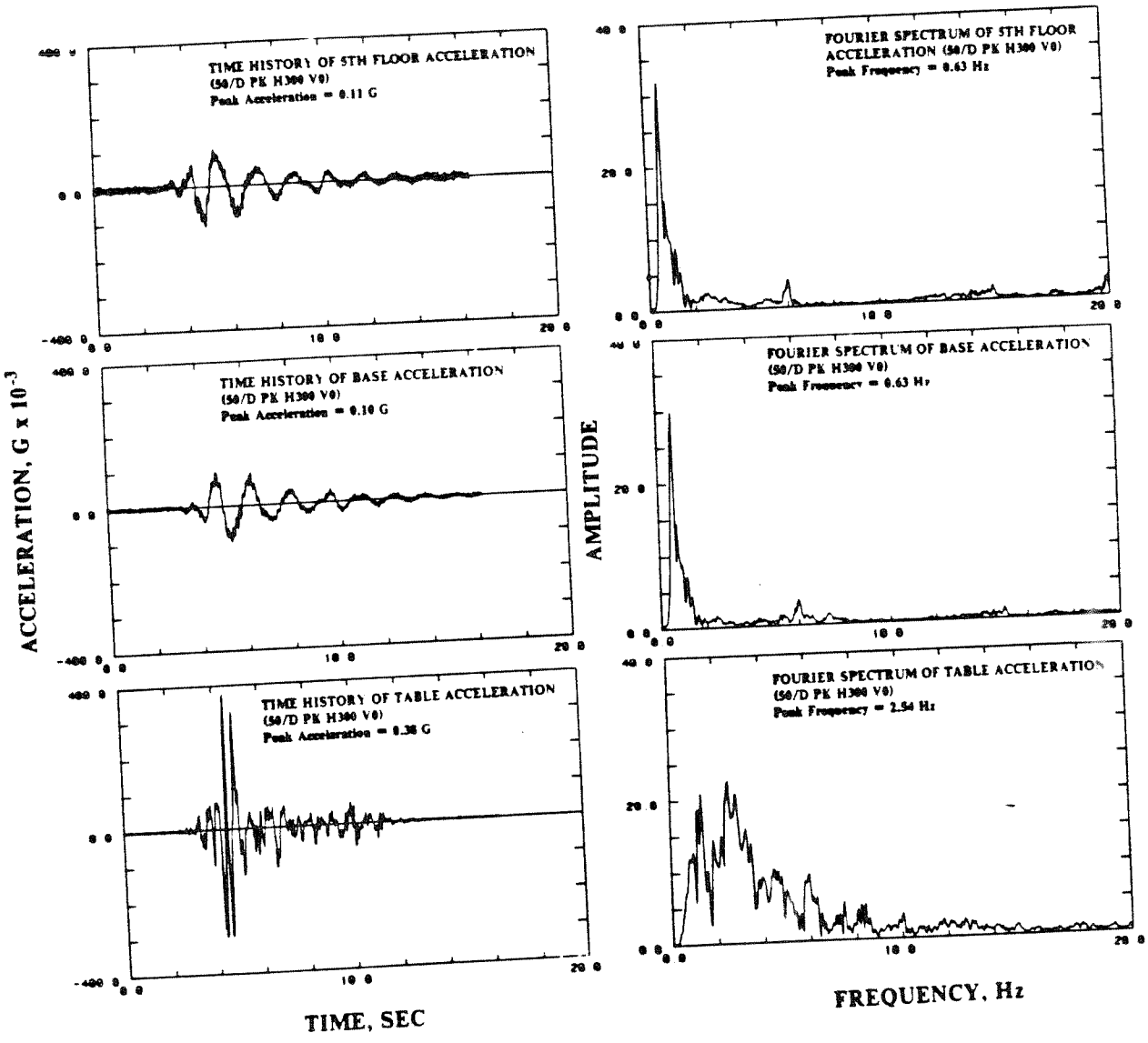

Figure 31 Acceleration Time Histories and Fourier Spectra of Frame in No-lead Bearing System under Parkfield Earthquake

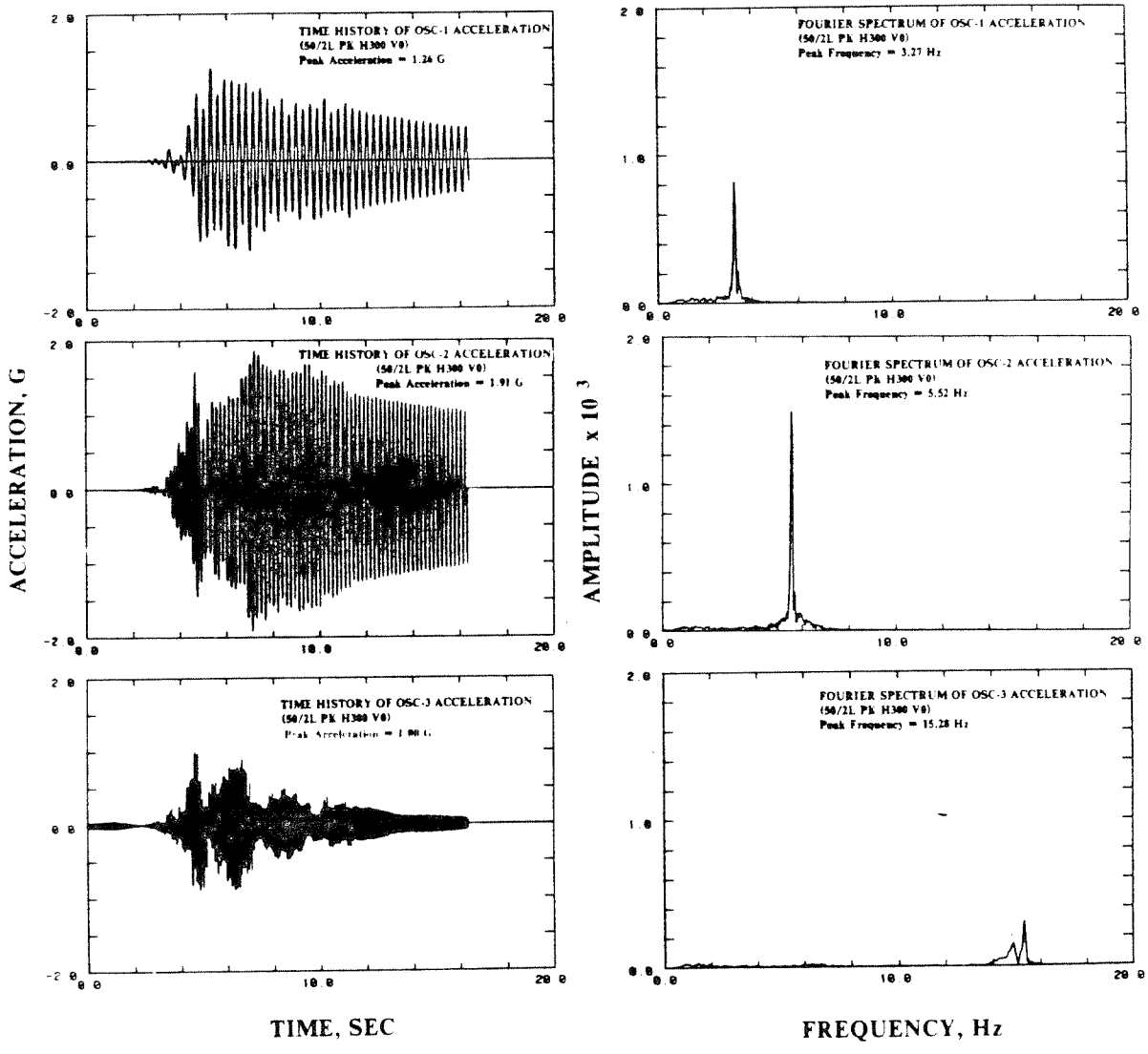

Figure 34 Acceleration Time Histories and Fourier Spectra of Oscillators on Lead Bearing System under Parkfield Earthquake

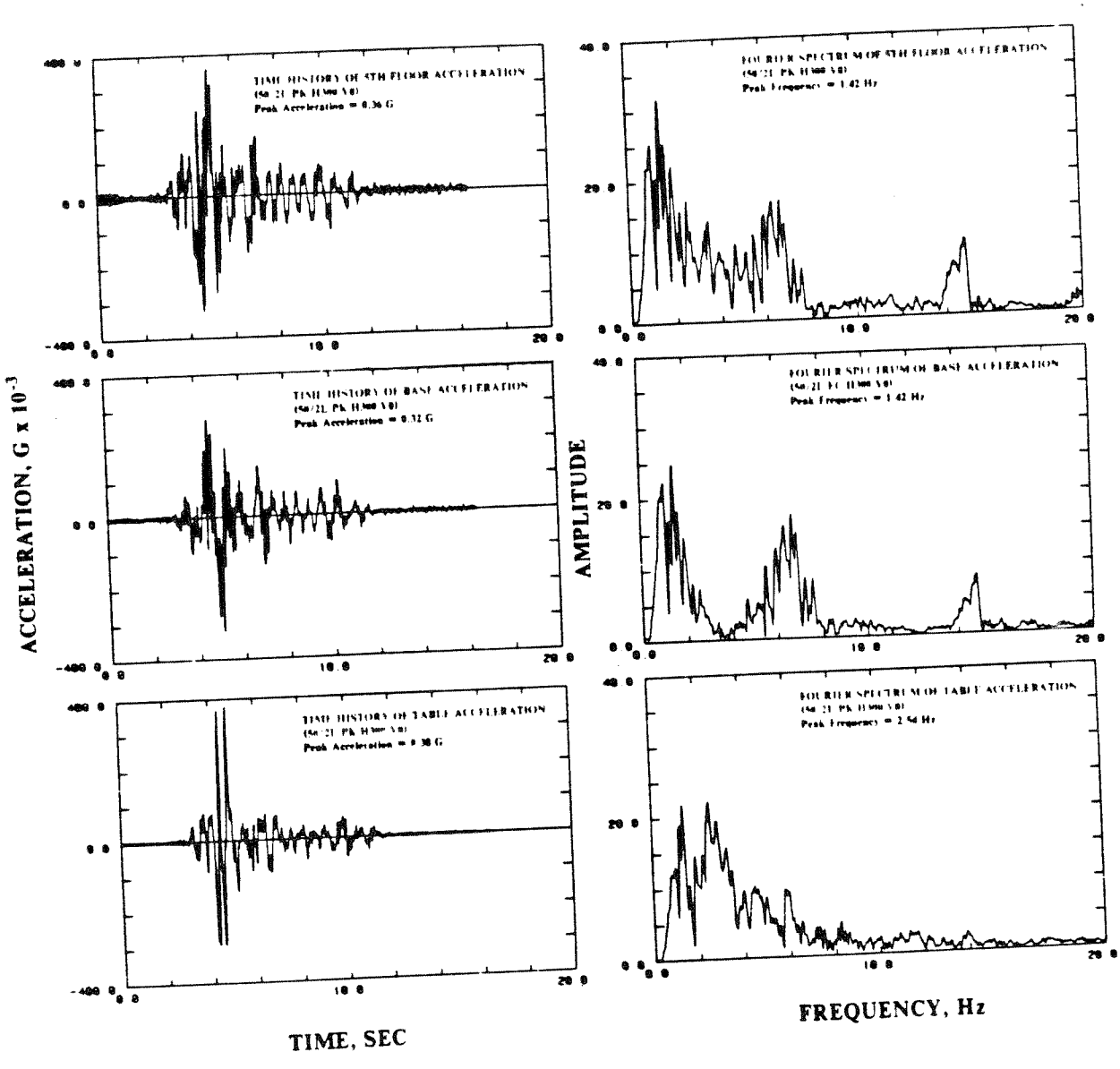

Figure 33 Acceleration Time Histories and Fourier Spectra of Frame in Lead Bearing System under Parkfield Earthquake

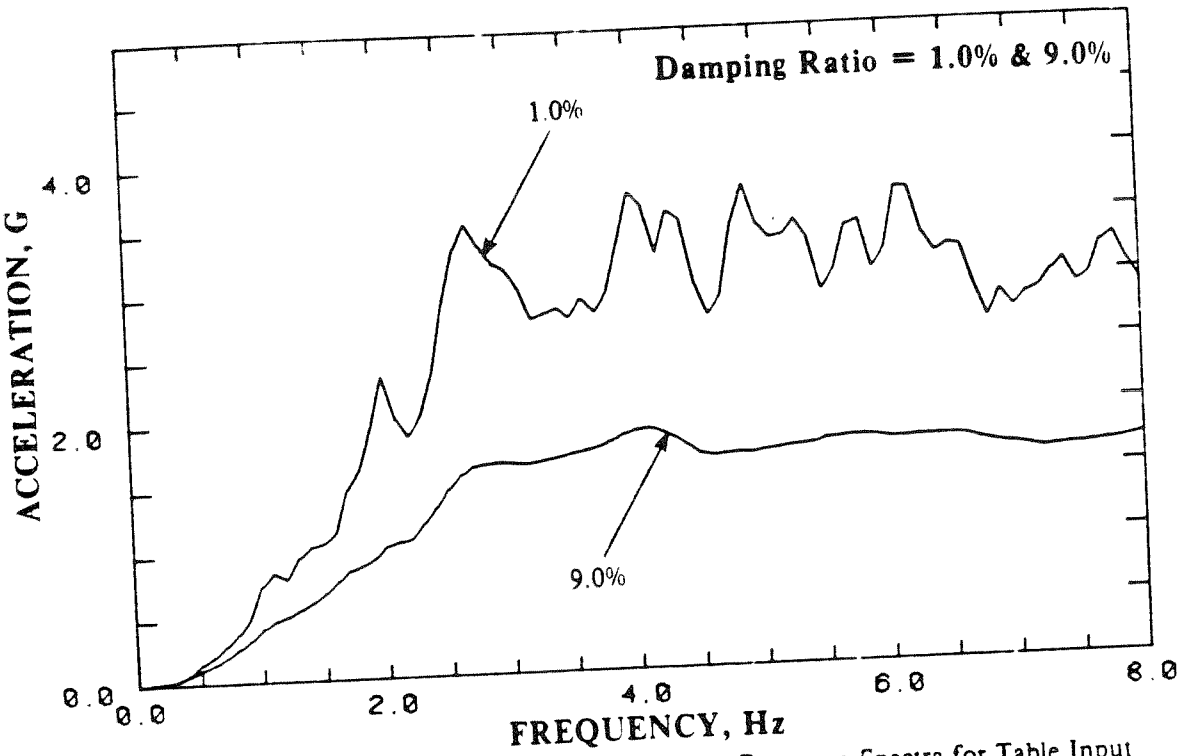

Figure 35 Average of Normalized Acceleration Response Spectra for Table Input in Fixed Base System

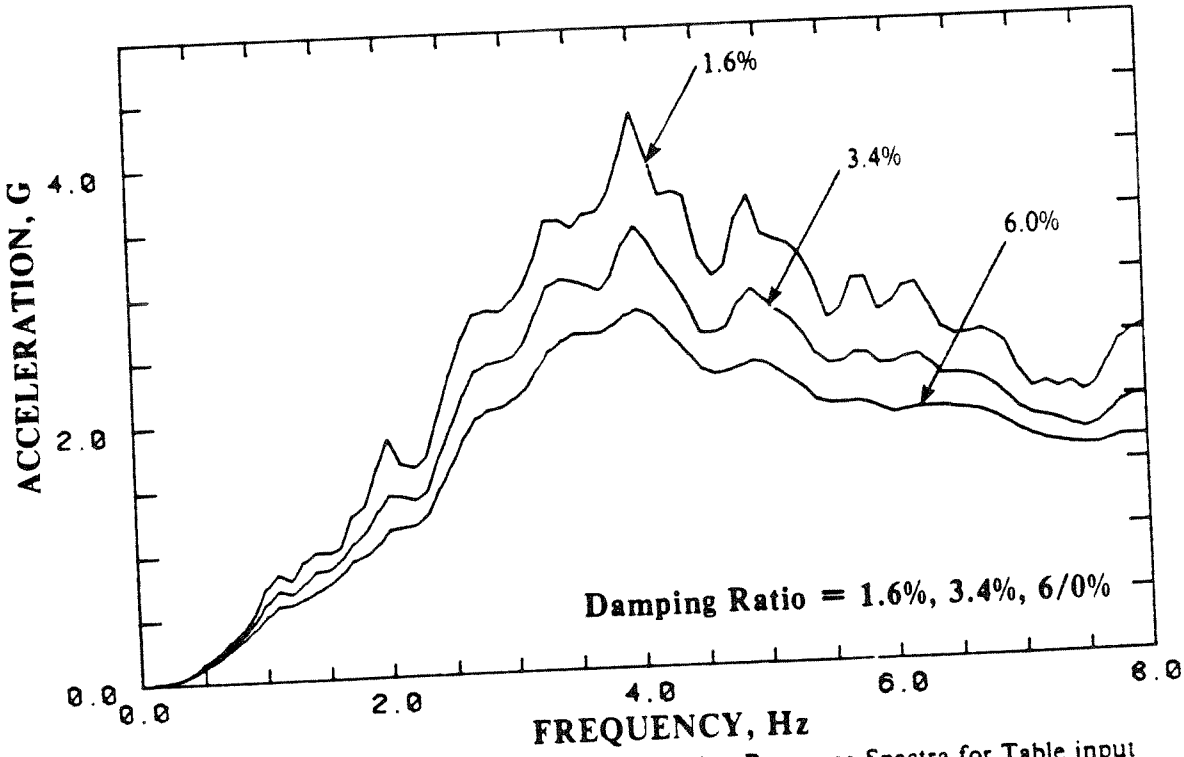

Figure 36 Average of Normalized Acceleration Response Spectra for Table input in No-lead Bearing system